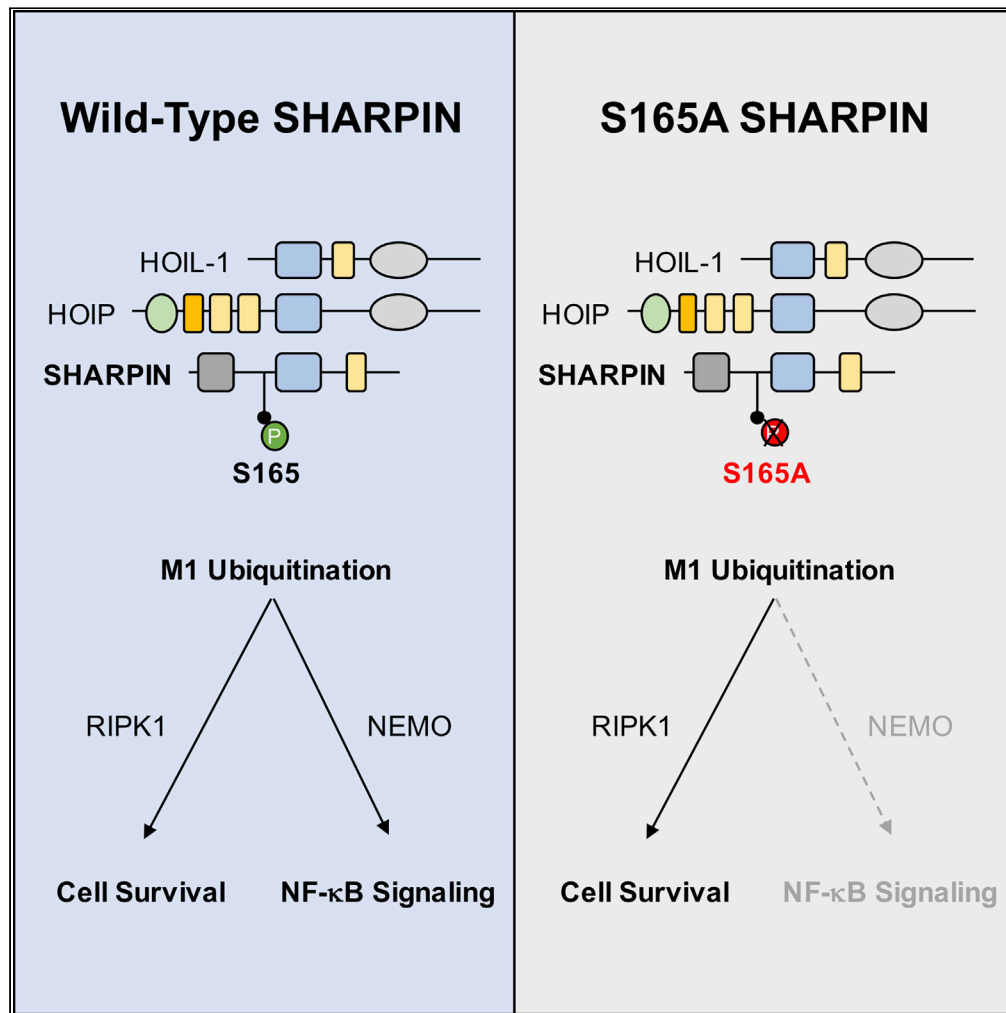## Article

Serine 165 phosphorylation of SHARPIN regulates the activation of NF-κB

An Thys, Kilian
Trillet, Sara
Rosińska, ...,
Franck Vérité,
Julie Gavard,
Nicolas Bidère

nicolas.bidere@inserm.fr

Highlights
Part of SHARPIN is
constitutively
phosphorylated on S165
in lymphoblastoid cells

SHARPIN S165
phosphorylation governs
TNFα-mediated linear
ubiquitination of NEMO

Mutation of S165 hinders
NF-κB activation

iScience

Article

Serine 165 phosphorylation of SHARPIN regulates the activation of NF-κB

An Thys,[1] Kilian Trillet,[1] Sara Rosińska,[1] Audrey Gayraud,[1] Tiphaine Douanne,[1] Yannic Danger,[2] Clotilde C.N. Renaud,[1] Luc Antigny,[1] Régis Lavigne,[3,4] Charles Pineau,[3,4] Emmanuelle Com,[3,4] Franck Vérité,[2] Julie Gavard,[1,5] and Nicolas Bidère[1,6,*]

Summary

The adaptor SHARPIN composes, together with the E3 ligases HOIP and HOIL1, the linear ubiquitin chain assembly complex (LUBAC). This enzymatic complex catalyzes and stamps atypical linear ubiquitin chains onto substrates to modify their fate and has been linked to the regulation of the NF-κB pathway downstream of most immunoreceptors, inflammation, and cell death. However, how this signaling complex is regulated is not fully understood. Here, we report that a portion of SHARPIN is constitutively phosphorylated on the serine at position 165 in lymphoblastoid cells and can be further induced following T cell receptor stimulation. Analysis of a phosphorylation-resistant mutant of SHARPIN revealed that this mark controls the linear ubiquitination of the NF-κB regulator NEMO and allows the optimal activation of NF-κB in response to TNFα. These results identify an additional layer of regulation of the LUBAC and unveil potential strategies to modulate its action.

Introduction

The linear ubiquitin chain assembly complex (LUBAC) is an enzymatic triad of the adaptor SHARPIN (SHANK-associated RH domain-interacting protein) and the E3 ligases HOIP (HOIL-1 interacting protein, also known as RNF31) and HOIL-1 (RanBP-type and C3HC4-type zinc finger-containing protein 1, also called RBCK1, HOIL-1L) (Gerlach et al., 2011; Ikeda et al., 2011; Tokunaga et al., 2011). This unique complex catalyzes the formation and attachment of atypical linear ubiquitin chains on substrates, thereby modifying their fate. The LUBAC acts as a linchpin by transducing signals from most immunoreceptors to nuclear factor (NF)-κB and therefore emerges as a key regulator of innate and adaptive immunity (Damgaard et al., 2012; Gerlach et al., 2011; Hostager et al., 2010; Ikeda et al., 2011; Inn et al., 2011; Karin and Greten, 2005; Kirisako et al., 2006; Shimizu et al., 2015; Tokunaga et al., 2009, 2011; Zak et al., 2011; Zhang et al., 2008). For instance, the binding of TNFα (tumor necrosis factor alpha) to its cognate receptor TNFR1 (TNF receptor 1) drives the recruitment of the LUBAC into the so-called complex I. By decorating key proteins such as RIPK1 (receptor-interacting protein 1 kinase) and NEMO (NF-κB essential modulator) with linear ubiquitin chains, the LUBAC counteracts cell death and favors downstream NF-κB signaling (Gerlach et al., 2011; Ikeda et al., 2011; Tokunaga et al., 2009, 2011). Mice deficient in *Sharpin*, *Hoip*, or *Hoil-1* are hallmarked by an exacerbated TNFα-induced cell death (Gerlach et al., 2011; Ikeda et al., 2011; Peltzer et al., 2014, 2018; Rickard et al., 2014; Tokunaga et al., 2011). The loss of LUBAC components destabilizes this TNFR signaling complex I and induces the assembly of cytosolic complex II, causing cell death by apoptosis or necroptosis (Gerlach et al., 2011; Peltzer et al., 2014; Rickard et al., 2014). Mice carrying a spontaneous *Sharpin*-null mutation (*cpdm*) develop multi-organ inflammation and chronic proliferative dermatitis, whereas HOIP and HOIL-1 deficiency is embryonically lethal (Gerlach et al., 2011; Ikeda et al., 2011; Peltzer et al., 2014, 2018; Rickard et al., 2014; Tokunaga et al., 2011). The LUBAC also functions downstream of antigen receptors to ensure the optimal activation of NF-κB, and this signaling pathway is pirated in the activated B cell-like subtype of diffuse large B cell lymphomas (ABC DLBCL) (Dubois et al., 2014; Satpathy et al., 2015; Teh et al., 2016; Yang et al., 2014). Accordingly, targeting of the LUBAC was shown to be toxic in ABC DLBCL, unveiling a contribution of this complex to lymphomagenesis (Dubois et al., 2014; Shaffer et al., 2012; Thys et al., 2018; Yang et al., 2014).

How the LUBAC is regulated continues to be elucidated. All members of the LUBAC have been reported to carry linear ubiquitin chains through auto-ubiquitination (Heger et al., 2018; Keusekotten et al., 2013).

[1]CRCINA, Inserm, CNRS, Université de Nantes, Université d'Angers, Nantes, France

[2]Etablissement Français du Sang (EFS), PFBI, Rennes, France

[3]Université de Rennes, Inserm, EHESP, Irset (Institut de recherche en santé, environnement et travail) - UMR_S 1085, Rennes, France

[4]Protim, Univ Rennes, Rennes, France

[5]Integrated Center for Oncology, ICO, St. Herblain, France

[6]Lead contact

*Correspondence: nicolas.bidere@inserm.fr

https://doi.org/10.1016/j.isci.2020.101939

Recently, Iwai and colleagues demonstrated that HOIL-1 E3 ligase mono-ubiquitinates the LUBAC, which causes HOIP to preferentially decorate the LUBAC with linear ubiquitin chains rather than other substrates (Fuseya et al., 2020). Linear auto-ubiquitination of the LUBAC can be removed by OTULIN (OTU deubiquitinase with linear linkage specificity) (Heger et al., 2018; Keusekotten et al., 2013). In addition, HOIP is processed upon TNFα- and TRAIL-induced apoptosis by caspases, with cleaved fragments displaying reduced NF-κB activation capabilities (Goto and Tokunaga, 2017; Joo et al., 2016). HOIP is also phosphorylated by MST1 (mammalian ste20-like kinase 1) in response to TNFα, and this modulates its E3 ligase activity, thereby attenuating NF-κB signaling (Lee et al., 2019). Three independent groups, including ours, showed that HOIL-1 is cleaved by the paracaspase MALT1 upon antigen receptor engagement and constitutively in ABC DLBCL to allow optimal activation of NF-κB (Douanne et al., 2016; Elton et al., 2016; Klein et al., 2015). Last, SHARPIN is decorated with lysine (K) 63 ubiquitin chains in mice on K312. This ubiquitination was shown to be important for the development of regulatory T cells (Park et al., 2016). However, what effect K63 ubiquitination of SHARPIN has on NF-κB signaling still remains an open question. Here, we demonstrate that a fraction of the LUBAC subunit SHARPIN is constitutively phosphorylated in lymphoblastoid cells, and this post-translational modification can be enhanced upon T cell receptor (TCR) engagement. We identify serine (S) 165 to be the primary phosphorylation site of SHARPIN and provide evidence of its crucial role for the optimal activation of NF-κB response to both TCR and TNFα stimulation.

Results and discussion
SHARPIN is a phosphoprotein

Western blotting analysis of SHARPIN, in human primary CD4^{+} and CD8^{+} cells, Jurkat cells, and DLBCL cell lines revealed that SHARPIN resolves as a doublet (Figures 1A, S1A, and S1B). The treatment of cell lysates with lambda phosphatase, which removes phosphate groups from serine, threonine, and tyrosine, effectively chased away the slow migration species of SHARPIN, suggesting phosphorylation (Figures 1A and S1A). Conversely, incubating cells with the phosphatase inhibitor calyculin A resulted in an increase in intensity of SHARPIN upper band, reinforcing the idea that SHARPIN is indeed phosphorylated (Figure 1A). Quantification of constitutive SHARPIN phosphorylation in numerous cell lines revealed that phospho-SHARPIN exists at various levels within different cell types, with lymphoid cells having a relatively high SHARPIN phosphorylation (Figures 1B and S1C–S1E). Hence, a fraction of SHARPIN is constitutively phosphorylated.

Next, we investigated whether stimuli, which employ SHARPIN, modify its phosphorylation. Mimicking TCR engagement with the DAG (diacylglycerol) analog PMA (phorbol 12-myristate 13-acetate) together with the protoionophore ionomycin (PI) increased the level of SHARPIN phosphorylation, which was efficiently removed by lambda phosphatase (Figures 1C and 1D). Similar results were observed in cells stimulated with antibodies to CD3 and CD28 (Figure S2A). This was further confirmed using a Phos-tag SDS-PAGE approach (Kinoshita et al., 2015) (Figure 1E). Of note, PMA alone, but not ionomycin alone, was sufficient to augment SHARPIN phosphorylation (Figures 1F and S2B). Importantly, TNFα had no overt effect on SHARPIN status (Figures 1F and S2B), suggesting that SHARPIN phosphorylation might be specifically increased upon TCR engagement. TCR stimulation culminates in the activation of NF-κB, ERK, JNK, and p38 (Samelson, 2011). To further explore the contribution of these signaling pathways, cells were first treated with the cell stress inducer anisomycin. Although this caused an activation of JNK and p38, SHARPIN phosphorylation remained even, excluding these two pathways (Figures 1F and S2B). We next assessed the role of ERK, whose activation was correlated with stimulation-mediated SHARPIN phosphorylation (Figures 1F and S2B). Incubating cells with the MEK1/2 inhibitor trametinib before treatment with PMA plus ionomycin or with antibodies to CD3 and CD28 hampered stimulation-induced SHARPIN phosphorylation, but did not prevent its basal constitutive mark (Figures 1G and S2C). By contrast, inhibition of the NF-κB pathway with the PKC inhibitor bisindolylmaleimide VIII (BIMVIII) had no overt effect (Figures 1G and S2C). These results suggest that the ERK pathway is selectively involved in TCR-mediated SHARPIN phosphorylation. To gain molecular insights, HOIP, SHARPIN, and ERK1-FLAG were overexpressed in HEKT293T cells. Co-immunoprecipitation of FLAG-tagged ERK1 revealed an interaction between SHARPIN and ERK1, which was lost in the absence of HOIP (Figure S2D). Likewise, SHARPIN phosphorylation could be induced by recombinant ERK applied to LUBAC isolated through pull down of the HOIL-1 subunit (Figures S2E and S2F). This suggests that SHARPIN phosphorylation by ERK requires the LUBAC. Altogether, our data favor a model in which at least two kinases are involved in the phosphorylation of SHARPIN: one yet unidentified kinase, which phosphorylates SHARPIN in resting conditions, and ERK1/2, which phosphorylates SHARPIN upon TCR engagement.
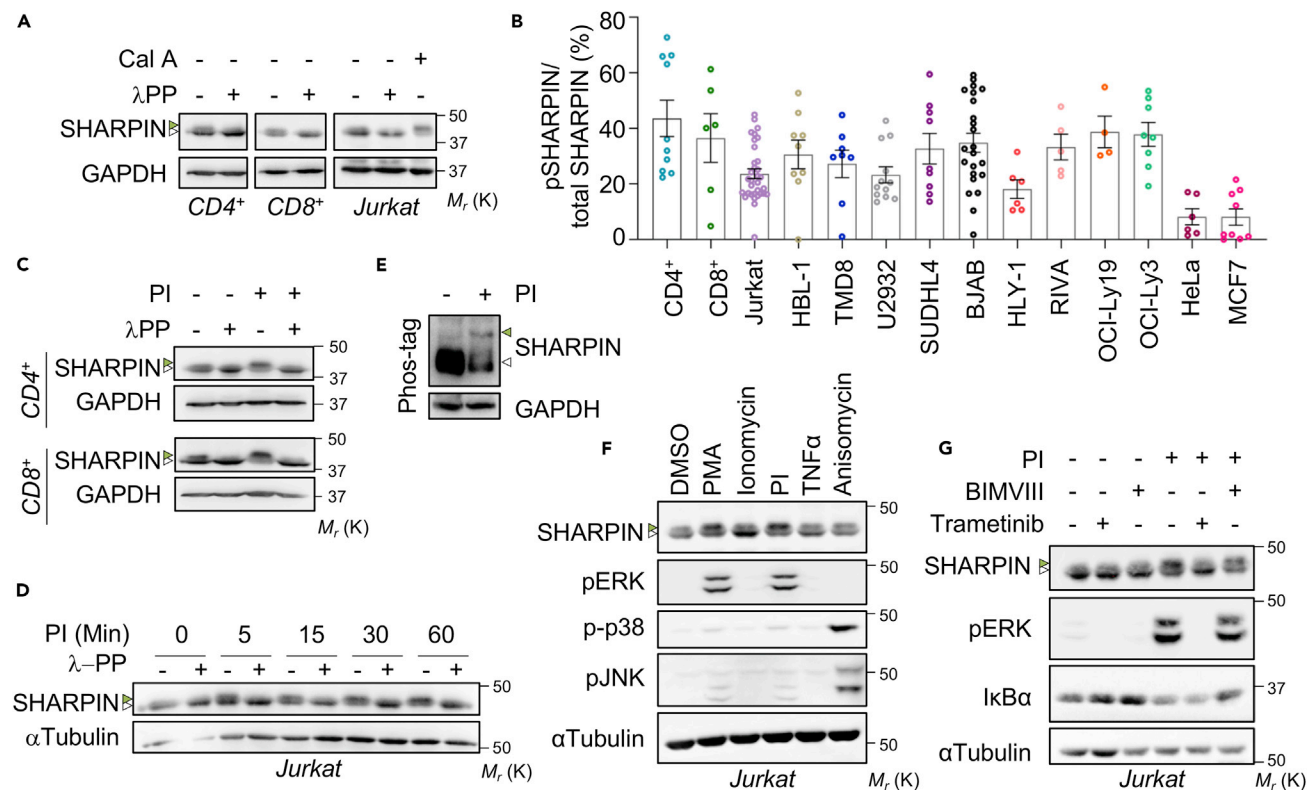
Figure 1. SHARPIN is a phosphoprotein

(A) Cell lysates from primary human CD4+ or CD8+ T lymphocytes and Jurkat cells were treated with lambda phosphatase (λPP) as indicated, and subjected to western blotting analysis. When indicated, Jurkat cells were treated with 50 nM calyculin A (Cal A) for 30 min before lysis. Green and white arrowheads indicate phosphorylated and unphosphorylated SHARPIN, respectively. Molecular weight markers (M_r) are indicated. GAPDH was used as a loading control.

(B) Densitometric analysis of the ratio between phosphorylated species of SHARPIN and SHARPIN in primary human T CD4+ cells, primary human T CD8+ T cells, Jurkat T cells, a panel of patient-derived diffuse large B cell lymphoma cell lines, and HeLa and MCF-7 cells. Each point represents the densitometric analysis of an individual blot ($n \geq 4$).

(C and D) Primary human CD4+ T and CD8+ T lymphocytes (C) and Jurkat cells (D) were stimulated for 30 min or as indicated with 20 ng/mL PMA plus 300 ng/mL ionomycin (PI). Lysates were prepared and treated or not with λPP, and western blotting analysis was performed as indicated. GAPDH or αTubulin served as loading control.

(E) Lysates from Jurkat cells treated as in (D) were resolved on a Phos-tag SDS-PAGE and analyzed by western blotting. GAPDH was used as loading control.

(F) Jurkat cells were treated with 20 ng/mL PMA, 300 ng/mL ionomycin, PMA plus ionomycin (PI), 10 ng/mL TNFα, or 12.5 μg/mL anisomycin for 30 min. Cell lysates were subjected to western blotting analysis. αTubulin served as loading control.

(G) Jurkat cells we pretreated for 1 h with 1 μM trametinib or 500 nM BIMVIII and subsequently stimulated and lysed as in (F). αTubulin was used as loading control. See also Figures S1 and S2. Western blotting data in (A) and (C–G) are representative of three or more independent experiments.

Serine 165 is the major phospho-acceptor site within SHARPIN

Mass spectrometry of SHARPIN, purified by SHARPIN immunoprecipitation of untreated Jurkat cells, was conducted to identify putative phosphorylation sites. In total, 20 peptides were recognized as SHARPIN, covering 45.5% of the protein sequence (Figure S3A). Five phosphorylated peptides were identified, and five phosphorylation sites were detected on S129, S131, S146, S165, and S312, with a probability of 65.20%, 50%, 92.44%, 100%, and 89.49%, respectively (Figures 2A and S3B). Out of the five serines identified, S165 and S312 were the most conserved ones across species (Figure 2B). To explore the details of SHARPIN phosphorylation, we engineered a stable Jurkat cell line deficient in *SHARPIN* using the CRISPR/Cas9 technology (Figures S3C and S3D). As previously reported (Gerlach et al., 2011; Ikeda et al., 2011; Rickard et al., 2014; Tokunaga et al., 2011), *SHARPIN*-deficient cells display compromised stability of the LUBAC subunits HOIP and HOIL-1, as well as diminished NF-κB activation (Figures S3D and S3E). *SHARPIN*-knockout Jurkat cells were subsequently reconstituted with an empty vector (EV), wild-type (WT) SHARPIN, or phospho-dead mutants of putative SHARPIN phosphorylation sites (S165A, S312A, S165A + S312A [2SA]). In both unstimulated and stimulated conditions, S165A-SHARPIN and
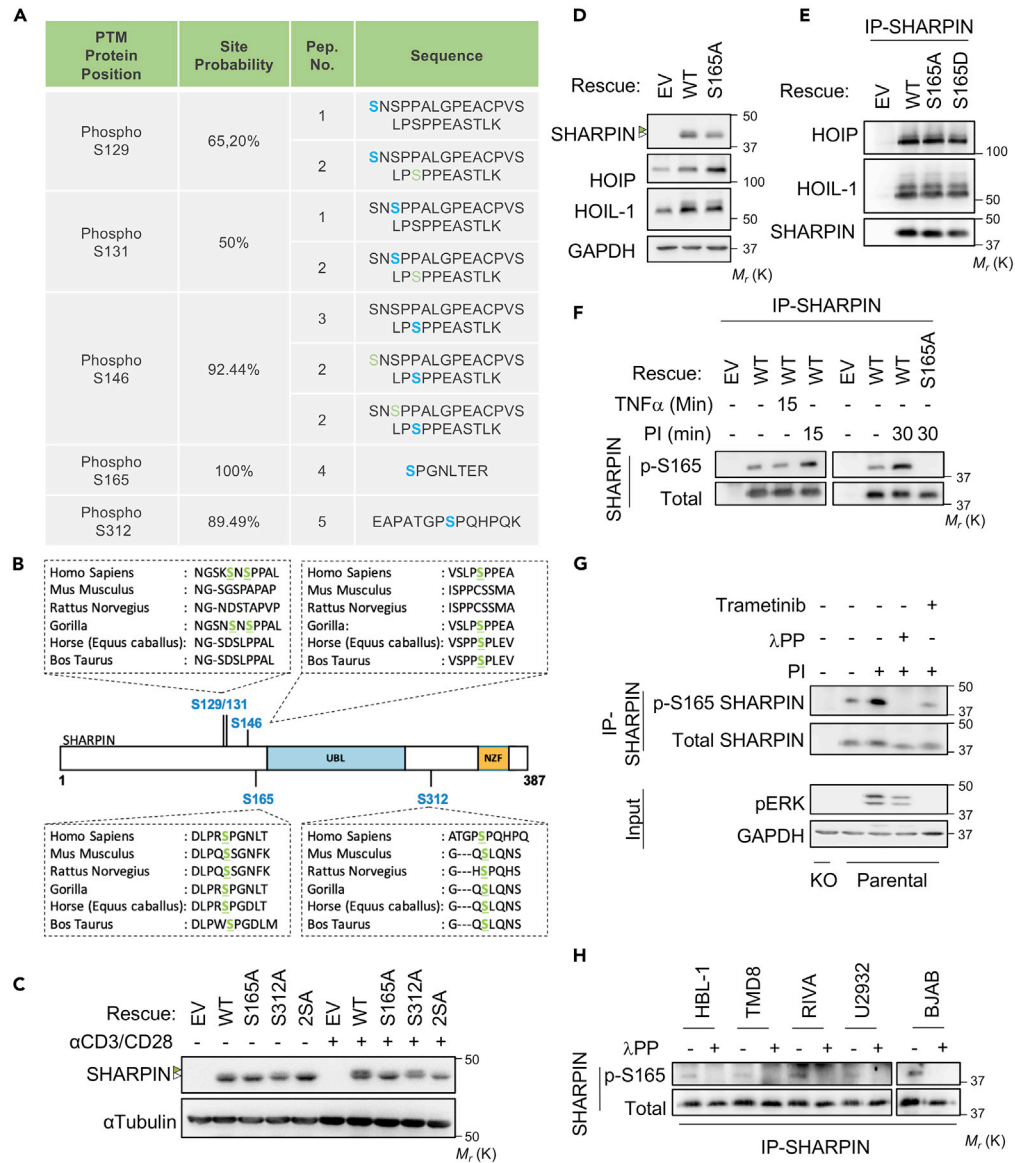
Figure 2. The serine residue of SHARPIN in position 165 is a major phosphorylation site

(A) Mass spectrometric analysis of immunoprecipitates prepared from Jurkat cell lysates with antibodies to SHARPIN identified phosphorylation sites. The identified peptides were validated with an false discovery rate <1% and a minimum score of 30. The peptide score was calculated in the Mascot search engine following $-10\log_{10}(p)$, where p is the absolute probability. The position of the post-translational modification in the protein (PTM), the modification site probability calculated in proline (site probability), the number of peptides identified, and the peptide sequence with the localization of the identified amino acid in blue and other amino acid modifications in green.

(B) Sequence alignment of the amino acids surrounding the serine (S) 129, S131, S146, S165, and S312 residues.

(C) Jurkat cells knockout for *SHARPIN* were engineered by CRISPR/Cas9. Cells were complemented with an empty vector (EV), or with wild-type (WT), S165A-, S312A-, or S165A plus S312A (2SA)-SHARPIN. Cells were stimulated for 30 min with antibodies to CD3 and CD28 (1 μg/mL each). Cell lysates were prepared and subjected to western blotting analysis. αTubulin was used as loading control. White and green symbols show SHARPIN and phosphorylated SHARPIN, respectively. Molecular weight markers (M_r) are indicated.

(D) Cell lysates from *SHARPIN*-knockout Jurkat cells reconstituted with an EV, WT-, or S165A-SHARPIN were prepared and analyzed by western blotting. GAPDH was used as loading control.

(E) Cell lysates from EV, WT-, S165A-, or S165D-SHARPIN reconstituted *SHARPIN*-knockout Jurkat cells were submitted to SHARPIN immunoprecipitation (IP) before western blotting analysis for LUBAC components. SHARPIN serves as loading control to ensure even pull down.

Figure 2. Continued

(F) Cells as in (D) were treated with 20 ng/mL PMA plus 300 ng/mL ionomycin (PI) or 10 ng/mL TNFα. Cells lysates were IP with antibodies specific to SHARPIN and subjected to western blotting analysis with a mouse antibody specific for p-S165-SHARPIN. Total SHARPIN served as control for IP.

(G) SHARPIN-knockout Jurkat cells reconstituted with an EV or parental Jurkat cells were pretreated with 1 μM trametinib for 1 h before stimulation with PI, as indicated. IP was performed as in (F), after which the IP beads were incubated with lambda phosphatase (λPP), as specified. Samples were subjected to western blotting analysis. Total SHARPIN functions as control for IP, and GAPDH is the loading control for the input.

(H) Lysates from indicated DLBCL cell lines were IP with antibodies to SHARPIN and treated, as indicated, with λPP. Samples were subsequently analyzed by western blotting. Total SHARPIN was used as loading control for IP. See also Figure S3. Western blotting data in (C–F and H) are representative of three or more independent experiments, and in (G) are representative of two independent experiments.

2SA-SHARPIN mutants had a faster migration in SDS-PAGE than WT- or S312A-SHARPIN (Figures 2C and S3F). This identifies S165 as the main phosphorylation site of SHARPIN. Rescuing Jurkat *SHARPIN* knockout cells with WT-, S165A- or phospho-mimetic S165D-SHARPIN resulted in a replenishment of the LUBAC components HOIP and HOIL-1, in a similar manner as the parental cells (Figures 2D and S3G). Accordingly, WT-, S165A-, and S165D-SHARPIN similarly bound to HOIP and HOIL-1 (Figure 2E). The LUBAC exists in mutually exclusive complexes, with the deubiquitinating enzymes CYLD or OTULIN (Elliott et al., 2014, 2016), and WT-, S165A-, or S165D-SHARPIN evenly bound to CYLD and OTULIN (Figure S3H). Hence, SHARPIN phosphorylation on S165 had seemingly no effect on the composition and stability of the LUBAC.

We next engineered a mouse phospho-specific S165 (p-S165) SHARPIN monoclonal antibody. Western blotting analysis, after immunoprecipitation of SHARPIN, confirmed that SHARPIN is constitutively phosphorylated on S165, and that this phosphorylation can be further induced upon PMA plus ionomycin activation, whereas it remains unaffected by TNFα stimulation (Figure 2F). As expected, no signal for p-S165 SHARPIN was detected in lysates from S165A-SHARPIN cells (Figure 2F). Moreover, the observed phospho-S165 SHARPIN signal was efficiently removed when samples were treated with lambda phosphatase (Figure 2G), thereby confirming the specificity of this antibody. Consistent with our previous results (Figures 1G and S2C), treatment with trametinib reduced SHARPIN phosphorylation upon stimulation with PMA plus ionomycin, while sparing basal constitutive signal (Figure 2G). Conversely, the addition of recombinant ERK to SHARPIN isolated by immunoprecipitation enhanced SHARPIN S165 phosphorylation (Figure S2I). Of note, SHARPIN phosphorylation on S165 was also found in a representative panel of DLBCL cell lines (Figure 2H). Altogether, this suggests that SHARPIN is constitutively phosphorylated on S165, and that ERK can further enhance this mark upon TCR stimulation.

SHARPIN phosphorylation contributes to the optimal activation of NF-κB

The LUBAC counteracts TNFα-induced cell death and conveys NF-κB signaling downstream of various immunoreceptors (Spit et al., 2019). TNFα stimulation drives the recruitment of the LUBAC to the TNFR1 complex I, where it stabilizes the complex and regulates NF-κB activation. It does so by attaching linear ubiquitin (methionine-1, M1) chains to components of the TNFR1 complex I, such as RIPK1 and the IκB kinase (IKK) complex regulator NEMO. Once activated, the IKK complex phosphorylates NF-κB inhibitors IκBs leading to their degradation. NF-κB is then free to translocate into the nucleus and exert its transcription factor function. Loss of LUBAC components leads to a switch from complex I to complex II, thereby inducing cell death by apoptosis or necroptosis (Gerlach et al., 2011; Peltzer et al., 2014; Rickard et al., 2014). We first studied the effect of SHARPIN phosphorylation on cell viability. As expected, the reconstitution of *SHARPIN* knockout cells with WT-SHARPIN reduced the enhanced cell loss observed in response to TNFα stimulation. The same was true in cells expressing S165A- or S165D-SHARPIN (Figure 3A). Accordingly, the recruitment of SHARPIN S165A to the TNFR1 complex I was normal, as was M1 ubiquitination at the TNFR1 receptor (Figures S4A and S4B). Likewise, TNFα stimulation did not drive any significant changes in total M1-linked ubiquitination or linear ubiquitination of RIPK1 (Figure 3B). Hence, SHARPIN phosphorylation on S165 appears dispensable for the recruitment of the LUBAC at the TNFR1 and for prevention of TNFα-mediated cell death.

We next investigated NF-κB activation. Upon TNFα or TCR stimulation, the transcription activity of NF-κB, as measured by a reporter luciferase assay, was reduced in *SHARPIN* knockout cells reconstituted with an empty vector, when compared with cells expressing WT- and S165D-SHARPIN (Figure 3C). However, this was not the case for S165A-SHARPIN (Figure 3C), unveiling a role for S165 phosphorylation in NF-κB
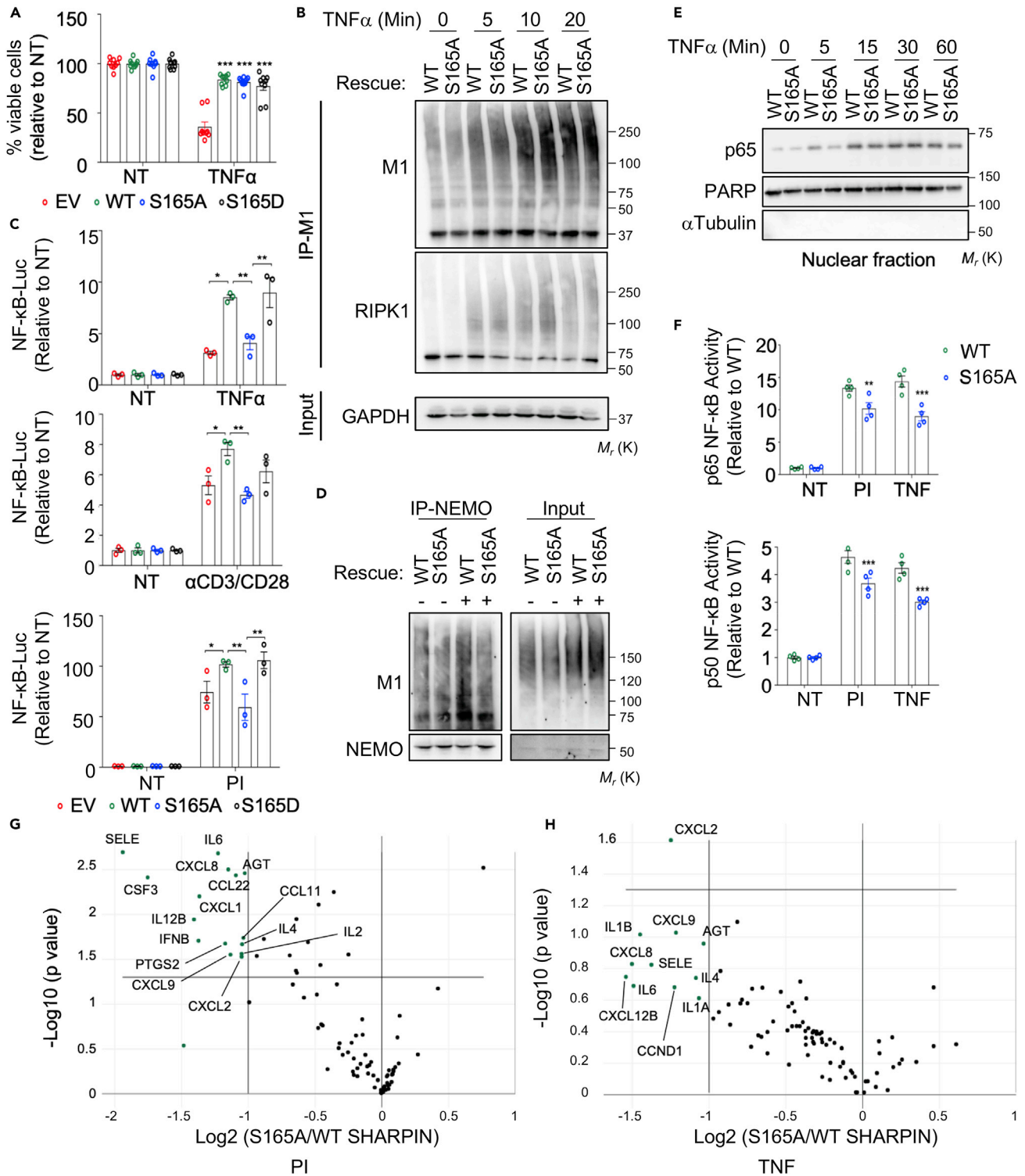
Figure 3. Serine 165 phosphorylation of SHARPIN is crucial for the optimal activation of NF-κB

(A) *SHARPIN*-knockout Jurkat cells expressing an empty vector (EV) or wild-type (WT-), S165A-, or S165D-SHARPIN were stimulated with 10 ng/mL TNFα for 24 h. Cell viability was assessed with CellTiter glo (mean ± SEM; ***p < 0.001 by two-way ANOVA, compared with EV). Graph represents three independent experiments performed in triplicate.

Figure 3. *Continued*

(B) WT- and S165A-expressing Jurkat cells were stimulated with 10 ng/mL TNFα, as indicated. Cell lysates were subjected to immunoprecipitation (IP) with antibodies against linear ubiquitin (M1) before western blotting analysis with the specified antibodies. Molecular weight markers (M_r) are indicated. GAPDH was used as loading control.

(C) NF-κB reporter luciferase assay in the indicated Jurkat cells treated for 6 h with 10 ng/mL TNFα, 1 μg/mL anti-CD3 plus 1 μg/mL anti-CD28, or with 20 ng/mL PMA plus 300 ng/mL ionomycin (PI) (mean ± SEM of triplicates; *p < 0.05, **p < 0.01 by two-way ANOVA, compared to WT). Shown is one experiment representative of three independent experiments.

(D) SHARPIN-knockout Jurkat cells stably expressing WT- or S165A-SHARPIN were stimulated for 10 min with 10 ng/mL TNFα. Cell lysates were subjected to NEMO immunoprecipitation (IP), and M1-ubiquitination was examined by western blotting analysis. NEMO was used as loading control.

(E) Nuclear fraction obtained by subcellular fractionation from *SHARPIN*-knockout Jurkat cells reconstituted with WT- or S165A-SHARPIN and stimulated with 10 ng/mL TNFα for the indicated time were analyzed by western blotting, as indicated. αTubulin and PARP serve as purity and loading controls.

(F) WT- or S165A-SHARPIN reconstituted Jurkat cells were stimulated with PI or TNFα for 30 min as in (C) before performing TransAM NF-κB activation assay for p65 and p50 NF-κB subunits (mean ± SEM; **p < 0.01, ***p < 0.001 by two-way ANOVA, compared with WT). Graphs represent two independent experiments done in duplicate.

(G and H) Volcano plot or RT^2 profiler PCR array of human NF-κB signaling targets for cells stimulated for 4 h with PI (G) or TNFα (H). Data represents biological triplicates. (G) Genes indicated on the volcano plot are significantly down regulated with a fold change >2 in cells expressing S165A-SHARPIN when compared with WT-SHARPIN. On (H), CXCL2 is significantly down regulated with a fold change >2, whereas other genes indicated are borderline significant in S165A-SHARPIN-expressing cells, compared with WT-SHARPIN. qPCR array was performed with biological triplicates.

See also Figure S4. Western blotting data in (B), (D), and (E) are representative of three or more independent experiments.

activation. Accordingly, less linear chains were found attached to NEMO in S165A-SHARPIN cells upon TNFα stimulation (Figure 3D). This led to an abnormal degradation of IκBα, visible at later time points of stimulation, combined with a delayed translocation of NF-κB p65 to the nucleus (Figures 3E, S4C, and S4D). Likewise, TransAM experiments showed reduced DNA binding of the NF-κB subunits p65 and p50 in S165A-SHARPIN-expressing cells upon TCR or TNFα stimulation (Figure 3F). In keeping with these results, PCR array of human NF-κB signaling targets showed significantly diminished expression of numerous cytokines (CSF3, IL12B, IFNBA, IL6, CXCL9, CCL22, IL2, and IL4) and chemokines (CXCLCL1, CXCL2, CXCL8, and CCL11) in S165A-SHARPIN-expressing cells treated with PMA and ionomycin (Figures 3G and S4E and Table S1). Similar trends were found when cells were stimulated with TNFα, albeit only the chemokine CXCL2 reached statistical significance (Figures 3H and S4F). It should be mentioned that compared with PMA plus ionomycin stimulation, induction of NF-κB target genes by TNFα was weaker. Nevertheless, we established that the phosphorylation of SHARPIN on S165 participates in NF-κB activation upon TCR and TNFα stimulation.

In summary, we have discovered that a part of SHARPIN is constitutively phosphorylated in lymphoblastoid cells and identified S165 as the main phospho-acceptor residue. We also provide evidence that SHARPIN is likely further phosphorylated on the S165 by ERK upon TCR ligation, but not in response to TNFα. Yet, the constitutive phosphorylation of SHARPIN is pivotal for the optimal activation of NF-κB in response to TCR engagement and TNFR ligation. This apparent dichotomy militates against a role for the inducible phosphorylation in NF-κB activation. It is therefore tempting to speculate that ERK-mediated phosphorylation of SHARPIN plays an independent function. Beside its crucial role in NF-κB signaling, a growing body of literature suggests that SHARPIN also acts as an inhibitor of the integrin adhesion receptors (De Franceschi et al., 2015; Pouwels et al., 2013; Rantala et al., 2011). Pouwels et al. demonstrated that SHARPIN locates at and controls the detachment of cellular protrusions called uropods in lymphocytes, and that this is essential for lymphocyte movement (Pouwels et al., 2013). As antigen receptor engagement delivers a stop signal to migrating T lymphocytes (Bousso and Robey, 2003; Dustin et al., 1997; Stoll, 2002), ERK-dependent SHARPIN phosphorylation may have an impact on cell adhesion and migration. This description of at least two kinases targeting the same site, with different outcomes is reminiscent of what has been shown for MLKL (mixed lineage kinase domain-like pseudokinase). MLKL acute phosphorylation by RIPK3 at T357 and S358 triggers necrotic cell death (Sun et al., 2012), whereas basal phosphorylation on the same sites by a yet-to-be-defined kinase promotes the generation of small extracellular vesicles (Yoon et al., 2017). Last, the LUBAC may exist in different complexes, with different binding partners (Elliott et al., 2014, 2016). One could therefore speculate that different kinases could target different LUBAC complexes, and consequently exert selective functions.

Although necessary for complete NF-κB activity, how SHARPIN phosphorylation precisely directs LUBAC activity is unclear. The basal S165 SHARPIN phosphorylation appeared dispensable for the recruitment of SHARPIN to the TNFR1, the linear ubiquitination of RIPK1, and for TNFα-induced cell death. However, we provide evidence that SHARPIN phosphorylation is selectively required for optimal M1-linked

ubiquitination of NEMO and subsequent activation of NF-κB. Although more work is required to better understand this added layer of complexity in the regulation of NF-κB transcription activity, this finding may also open additional avenues for therapeutic prospects of aggressive lymphoma, such as ABC DLBCL, for which the LUBAC and NF-κB activation is pivotal for survival (Dubois et al., 2014; Yang et al., 2014). *Hoip* and *Sharpin* deficiency in mice results in embryonic lethality and multiorgan inflammation, respectively, which is driven by aberrant TNFα-induced cell death (Compagno et al., 2009; Davis et al., 2001; Peltzer et al., 2014; Rickard et al., 2014; Seymour et al., 2007). Directly interfering with SHARPIN phosphorylation for treatment may therefore circumvent the pitfall of inducing autoinflammatory diseases while targeting the NF-κB pathway specifically. The identification of the kinase responsible for constitutive SHARPIN phosphorylation will therefore be paramount to our future research.

Limitations of the study

Our study reveals a role for SHARPIN S165 phosphorylation on NF-κB activation in Jurkat T lymphocytes. Although this cellular model constitutes a well-accepted and relevant system to study TCR and TNFα signaling (Abraham and Weiss, 2004), we did not confront these findings with primary lymphocytes or with *in vivo* models. Whether SHARPIN phosphorylation impacts other cell lineages remains to be tested. The LUBAC functions as a gateway for NF-κB signaling downstream variety of immunoreceptors, and future work will be aimed at defining the contribution of SHARPIN phosphorylation. In addition, how exactly this mark marshals optimal NF-κB activation on a molecular standpoint remains unclear. For instance, it would be interesting to explore if the IKK complex is normally recruited to the TNFR1 complex I and phosphorylated in SHARPIN S165A-expressing cells. Last, although we essentially focused on the constitutive phosphorylation of SHARPIN, our results support the idea that ERK exacerbates this mark upon TCR stimulation. This hypothesis relies on chemical inhibition with trametinib and *in vitro* kinase assay. Combined targeting of ERK1 and ERK2 was not sufficient, in our hands, to achieve complete depletion of these abundant kinases, making interpretation of the data complicated and necessitating further investigation.

Resource availability

Lead contact

Further information and requests for resources and reagents should be directed to and will be fulfilled by the Lead Contact, Nicolas Bidère (nicolas.bidere@inserm.fr).

Materials availability

All reagents generated in this study are available from the Lead Contact with a completed Material Transfer Agreement.

Data and code availability

This study did not generate large-scale datasets. Raw data of this article are available from the Lead Contact upon request.

Methods

All methods can be found in the accompanying Transparent methods supplemental file.

Supplemental information

Supplemental Information can be found online at https://doi.org/10.1016/j.isci.2020.101939.

Author contributions

A.T.: Conceptualization, Methodology, Formal Analysis, Investigation, Writing – Original Draft, Visualization, and Funding Acquisition. K.T., S.R., A.G., T.D., C.R., L.A., and R.L.: Investigation. Y.D., and F.V.: Resources. E.C.: Methodology, Formal Analysis, Investigation. C.P.: Methodology. J.G.: Writing – Review and Editing, Supervision, and Funding Acquisition. N.B.: Conceptualization, Methodology, Investigation, Writing – Original Draft, Visualization, and Funding Acquisition.

Declaration of interests

The authors declare no competing interests.

References

Abraham, R.T., and Weiss, A. (2004). Jurkat T cells and development of the T-cell receptor signalling paradigm. Nat. Rev. Immunol. 4, 301–308.

Bousso, P., and Robey, E. (2003). Dynamics of CD8+ T cell priming by dendritic cells in intact lymph nodes. Nat. Immunol. 4, 579–585.

Compagno, M., Lim, W.K., Grunn, A., Nandula, S.V., Brahmachary, M., Shen, Q., Bertoni, F., Ponzoni, M., Scandurra, M., Califano, A., et al. (2009). Mutations of multiple genes cause deregulation of NF-κB in diffuse large B-cell lymphoma. Nature 459, 717–721.

Damgaard, R.B., Nachbur, U., Yabal, M., Wong, W.W.-L., Fiil, B.K., Kastirr, M., Rieser, E., Rickard, J.A., Bankovacki, A., Peschel, C., et al. (2012). The ubiquitin ligase XIAP recruits LUBAC for NOD2 signaling in inflammation and innate immunity. Mol. Cell 46, 746–758.

Davis, R.E., Brown, K.D., Siebenlist, U., and Staudt, L.M. (2001). Constitutive nuclear factor κB activity is required for survival of activated B cell–like diffuse large B cell lymphoma cells. J. Exp. Med. 194, 1861–1874.

De Franceschi, N., Peuhu, E., Parsons, M., Rissanen, S., Vattulainen, I., Salmi, M., Ivaska, J., and Pouwels, J. (2015). Mutually exclusive roles of SHARPIN in integrin inactivation and NF-κB signaling. PLoS One 10, e0143423.

Douanne, T., Gavard, J., and Bidère, N. (2016). The paracaspase MALT1 cleaves the LUBAC subunit HOIL1 during antigen receptor signaling. J. Cell Sci. 129, 1775–1780.

Dubois, S.M., Alexia, C., Wu, Y., Leclair, H.M., Leveau, C., Schol, E., Fest, T., Tarte, K., Chen, Z.J., Gavard, J., et al. (2014). A catalytic-independent role for the LUBAC in NF-kappaB activation upon antigen receptor engagement and in lymphoma cells. Blood 123, 2199–2203.

Dustin, M.L., Bromley, S.K., Kan, Z., Peterson, D.A., and Unanue, E.R. (1997). Antigen receptor engagement delivers a stop signal to migrating T lymphocytes. Proc. Natl. Acad. Sci. U S A 94, 3909–3913.

Elliott, P.R., Nielsen, S.V., Marco-Casanova, P., Fiil, B.K., Keusekotten, K., Mailand, N., Freund, S.M.V., Gyrd-Hansen, M., and Komander, D. (2014). Molecular basis and regulation of OTULIN-LUBAC interaction. Mol. Cell 54, 335–348.

Elliott, P.R., Leske, D., Hrdinka, M., Bagola, K., Fiil, B.K., McLaughlin, S.H., Wagstaff, J., Volkmar, N., Christianson, J.C., Kessler, B.M., et al. (2016). SPATA2 links CYLD to LUBAC, activates CYLD, and controls LUBAC signaling. Mol. Cell 63, 990–1005.

Elton, L., Carpentier, I., Staal, J., Driege, Y., Haegman, M., and Beyaert, R. (2016). MALT1 cleaves the E3 ubiquitin ligase HOIL-1 in activated T cells, generating a dominant negative inhibitor of LUBAC-induced NF-κB signaling. FEBS J. 283, 403–412.

Fuseya, Y., Fujita, H., Kim, M., Ohtake, F., Nishide, A., Sasaki, K., Saeki, Y., Tanaka, K., Takahashi, R., and Iwai, K. (2020). The HOIL-1L ligase modulates immune signalling and cell death via monoubiquitination of LUBAC. Nat. Cell Biol. 22, 663–673.

Gerlach, B., Cordier, S.M., Schmukle, A.C., Emmerich, C.H., Rieser, E., Haas, T.L., Webb, A.I., Rickard, J.A., Anderton, H., Wong, W.W.-L., et al. (2011). Linear ubiquitination prevents inflammation and regulates immune signalling. Nature 471, 591–596.

Goto, E., and Tokunaga, F. (2017). Decreased linear ubiquitination of NEMO and FADD on apoptosis with caspase-mediated cleavage of HOIP. Biochem. Biophys. Res. Commun. 485, 152–159.

Heger, K., Wickliffe, K.E., Ndoja, A., Zhang, J., Murthy, A., Dugger, D.L., Maltzman, A., de Sousa e Melo, F., Hung, J., Zeng, Y., et al. (2018). OTULIN limits cell death and inflammation by deubiquitinating LUBAC. Nature 559, 120–124.

Hostager, B.S., Fox, D.K., Whitten, D., Wilkerson, C.G., Eipper, B.A., Francone, V.P., Rothman, P.B., and Colgan, J.D. (2010). HOIL-1L interacting protein (HOIP) as an NF-κB regulating component of the CD40 signaling complex. PLoS One 5, e11380.

Ikeda, F., Deribe, Y.L., Skånland, S.S., Stieglitz, B., Grabbe, C., Franz-Wachtel, M., van Wijk, S.J.L.,

Goswami, P., Nagy, V., Terzic, J., et al. (2011). SHARPIN forms a linear ubiquitin ligase complex regulating NF-kB activity and apoptosis. Nature 471, 637–641.

Inn, K.-S., Gack, M.U., Tokunaga, F., Shi, M., Wong, L.-Y., Iwai, K., and Jung, J.U. (2011). Linear ubiquitin assembly complex negatively regulates RIG-I- and TRIM25-mediated type I Interferon induction. Mol. Cell 41, 354–365.

Joo, D., Tang, Y., Blonska, M., Jin, J., Zhao, X., and Lin, X. (2016). Regulation of linear ubiquitin chain assembly complex by caspase-mediated cleavage of RNF31. Mol. Cell. Biol. 36, 3010–3018.

Karin, M., and Greten, F.R. (2005). NF-κB: linking inflammation and immunity to cancer development and progression. Nat. Rev. Immunol. 5, 749–759.

Keusekotten, K., Elliott, P.R., Glockner, L., Fiil, B.K., Damgaard, R.B., Kulathu, Y., Wauer, T., Hospenthal, M.K., Gyrd-Hansen, M., Krappmann, D., et al. (2013). OTULIN antagonizes LUBAC signaling by specifically hydrolyzing Met1-linked polyubiquitin. Cell 153, 1312–1326.

Kinoshita, E., Kinoshita-Kikuta, E., and Koike, T. (2015). Advances in Phos-tag-based methodologies for separation and detection of the phosphoproteome. Biochim. Biophys. Acta 1854, 601–608.

Kirisako, T., Kamei, K., Murata, S., Kato, M., Fukumoto, H., Kanie, M., Sano, S., Tokunaga, F., Tanaka, K., and Iwai, K. (2006). A ubiquitin ligase complex assembles linear polyubiquitin chains. EMBO J. 25, 4877–4887.

Klein, T., Fung, S.-Y., Renner, F., Blank, M.A., Dufour, A., Kang, S., Bolger-Munro, M., Scurll, J.M., Priatel, J.J., Schweigler, P., et al. (2015). The paracaspase MALT1 cleaves HOIL1 reducing linear ubiquitination by LUBAC to dampen lymphocyte NF-κB signalling. Nat. Commun. 6, 8777.

Lee, I.Y., Lim, J.M., Cho, H., Kim, E., Kim, Y., Oh, H.-K., Yang, W.S., Roh, K.-H., Park, H.W., Mo, J.-S., et al. (2019). MST1 negatively regulates TNFα-induced NF-κB signaling through modulating LUBAC activity. Mol. Cell 73, 1138–1149.e6.

Park, Y., Jin, H., Lopez, J., Lee, J., Liao, L., Elly, C., and Liu, Y.-C. (2016). SHARPIN controls regulatory T cells by negatively modulating the T cell antigen receptor complex. Nat. Immunol. 17, 286–296.

Peltzer, N., Rieser, E., Taraborrelli, L., Draber, P., Darding, M., Pernaute, B., Shimizu, Y., Sarr, A., Draberova, H., Montinaro, A., et al. (2014). HOIP deficiency causes embryonic lethality by aberrant TNFR1-mediated endothelial cell death. Cell Rep. 9, 153–165.

Peltzer, N., Darding, M., Montinaro, A., Draber, P., Draberova, H., Kupka, S., Rieser, E., Fisher, A., Hutchinson, C., Taraborrelli, L., et al. (2018). LUBAC is essential for embryogenesis by preventing cell death and enabling haematopoiesis. Nature 557, 112–117.

Pouwels, J., De Franceschi, N., Rantakari, P., Auvinen, K., Karikoski, M., Mattila, E., Potter, C., Sundberg, J.P., Hogg, N., Gahmberg, C.G., et al. (2013). SHARPIN regulates uropod detachment in migrating lymphocytes. Cell Rep. 5, 619–628.

Rantala, J.K., Pouwels, J., Pellinen, T., Veltel, S., Laasola, P., Mattila, E., Potter, C.S., Duffy, T., Sundberg, J.P., Kallioniemi, O., et al. (2011). SHARPIN is an endogenous inhibitor of β1-integrin activation. Nat. Cell Biol. 13, 1315–1324.

Rickard, J.A., Anderton, H., Etemadi, N., Nachbur, U., Darding, M., Peltzer, N., Lalaoui, N., Lawlor, K.E., Vanyai, H., Hall, C., et al. (2014). TNFR1-dependent cell death drives inflammation in Sharpin-deficient mice. Elife 3, e03464.

Samelson, L.E. (2011). Immunoreceptor signaling. Cold Spring Harb. Perspect. Biol. 3, a011510.

Satpathy, S., Wagner, S.A., Beli, P., Gupta, R., Kristiansen, T.A., Malinova, D., Francavilla, C., Tolar, P., Bishop, G.A., Hostager, B.S., et al. (2015). Systems-wide analysis of BCR signalosomes and downstream phosphorylation and ubiquitylation. Mol. Syst. Biol. 11, 810.

Seymour, R.E., Hasham, M.G., Cox, G.A., Shultz, L.D., Hogenesch, H., Roopenian, D.C., and Sundberg, J.P. (2007). Spontaneous mutations in the mouse Sharpin gene result in multiorgan inflammation, immune system dysregulation and dermatitis. Genes Immun. 8, 416–421.

Shaffer, A.L., 3rd, Young, R.M., and Staudt, L.M. (2012). Pathogenesis of human B cell lymphomas. Annu. Rev. Immunol. 30, 565–610.

Shimizu, Y., Taraborrelli, L., and Walczak, H. (2015). Linear ubiquitination in immunity. Immunol. Rev. 266, 190–207.

Spit, M., Rieser, E., and Walczak, H. (2019). Linear ubiquitination at a glance. J. Cell Sci. 132, jcs208512.

Stoll, S. (2002). Dynamic imaging of T cell-dendritic cell interactions in lymph nodes. Science 296, 1873–1876.

Sun, L., Wang, H., Wang, Z., He, S., Chen, S., Liao, D., Wang, L., Yan, J., Liu, W., Lei, X., et al. (2012). Mixed lineage kinase domain-like protein mediates necrosis signaling downstream of RIP3 kinase. Cell 148, 213–227.

Teh, C.E., Lalaoui, N., Jain, R., Policheni, A.N., Heinlein, M., Alvarez-Diaz, S., Sheridan, J.M., Rieser, E., Deuser, S., Darding, M., et al. (2016). Linear ubiquitin chain assembly complex coordinates late thymic T-cell differentiation and regulatory T-cell homeostasis. Nat. Commun. 7, 13353.

Thys, A., Douanne, T., and Bidere, N. (2018). Post-translational modifications of the CARMA1-BCL10-MALT1 complex in lymphocytes and

activated B-cell like subtype of diffuse large B-cell lymphoma. Front. Oncol. 8, 498.

Tokunaga, F., Sakata, S., Saeki, Y., Satomi, Y., Kirisako, T., Kamei, K., Nakagawa, T., Kato, M., Murata, S., Yamaoka, S., et al. (2009). Involvement of linear polyubiquitylation of NEMO in NF-κB activation. Nat. Cell Biol. 11, 123–132.

Tokunaga, F., Nakagawa, T., Nakahara, M., Saeki, Y., Taniguchi, M., Sakata, S., Tanaka, K., Nakano, H., and Iwai, K. (2011). SHARPIN is a component of the NF-kB-activating linear ubiquitin chain assembly complex. Nature 471, 633–636.

Yang, Y., Schmitz, R., Mitala, J., Whiting, A., Xiao, W., Ceribelli, M., Wright, G.W., Zhao, H., Yang, Y., Xu, W., et al. (2014). Essential role of the linear ubiquitin chain assembly complex in lymphoma revealed by rare germline polymorphisms. Cancer Discov. 4, 480–493.

Yoon, S., Kovalenko, A., Bogdanov, K., and Wallach, D. (2017). MLKL, the protein that mediates necroptosis, also regulates endosomal trafficking and extracellular vesicle generation. Immunity 47, 51–65.e7.

Zak, D.E., Schmitz, F., Gold, E.S., Diercks, A.H., Peschon, J.J., Valvo, J.S., Niemisto, A., Podolsky, I., Fallen, S.G., Suen, R., et al. (2011). Systems analysis identifies an essential role for SHANK-associated RH domain-interacting protein (SHARPIN) in macrophage Toll-like receptor 2 (TLR2) responses. Proc. Natl. Acad. Sci. U S A 108, 11536–11541.

Zhang, M., Tian, Y., Wang, R.-P., Gao, D., Zhang, Y., Diao, F.-C., Chen, D.-Y., Zhai, Z.-H., and Shu, H.-B. (2008). Negative feedback regulation of cellular antiviral signaling by RBCK1-mediated degradation of IRF3. Cell Res. 18, 1096–1104.

Supplemental Information

Serine 165 phosphorylation of SHARPIN

regulates the activation of NF-κB

An Thys, Kilian Trillet, Sara Rosińska, Audrey Gayraud, Tiphaine Douanne, Yannic Danger, Clotilde C.N. Renaud, Luc Antigny, Régis Lavigne, Charles Pineau, Emmanuelle Com, Franck Vérité, Julie Gavard, and Nicolas Bidère
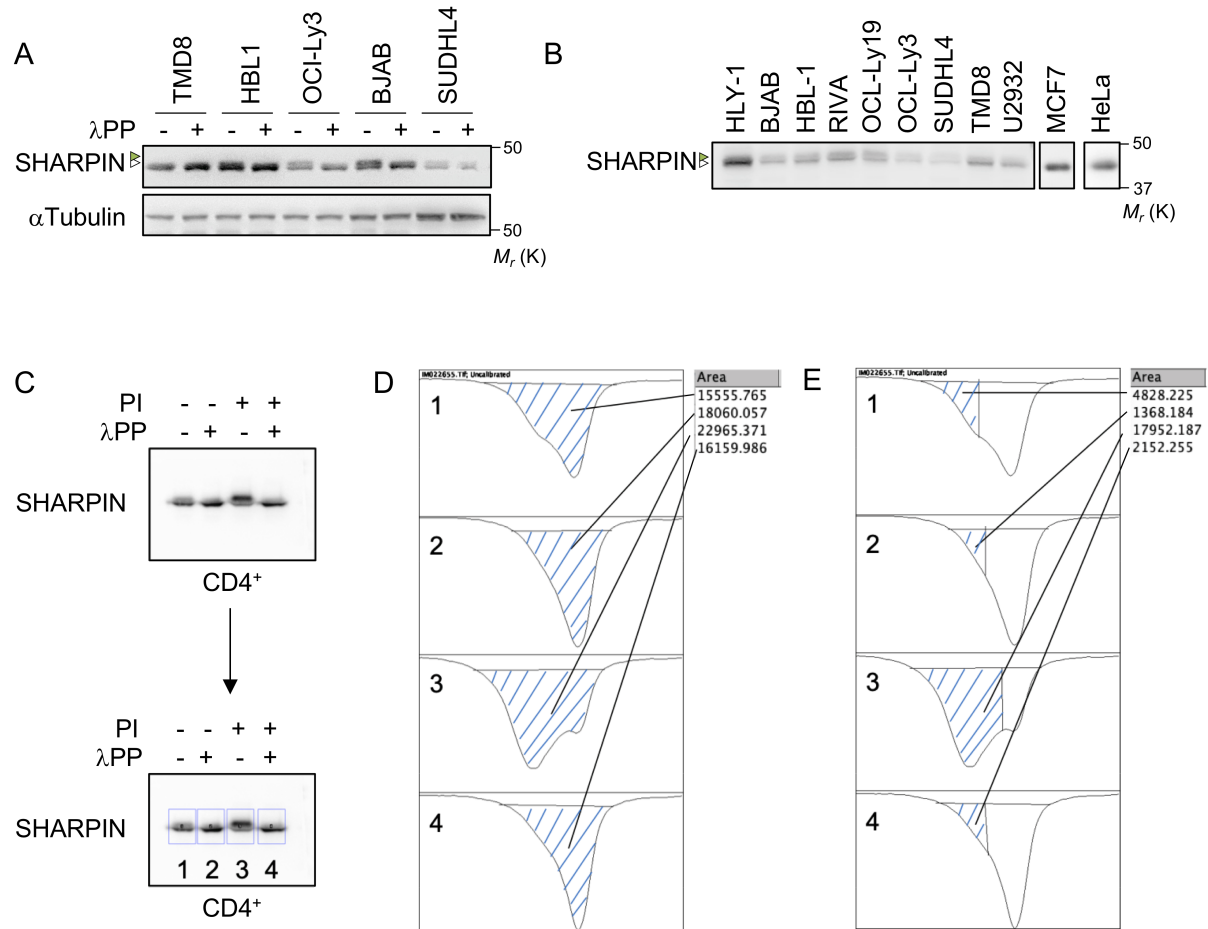
Figure S1. Analysis of SHARPIN Phosphorylation. Related to Figure 1

(A and B) Western blotting analysis of a panel of patient-derived diffuse large B-cell lymphoma (DLBCL) cell lines, MCF7 and HeLa cells. In (A) cell lysates were treated with lambda phosphatase (λPP) when indicated, and subjected to Western blotting analysis. Green and white arrowheads indicate phosphorylated and unphosphorylated SHARPIN, respectively. Molecular weight markers (M_r) are indicated. Data are representative of three or more independent experiments.

(C-E) Procedure for densitometric analysis of SHARPIN phosphorylation. (C) For each condition, lanes were selected using the "gels" function of ImageJ in the drop-down menu "Analyse". (D) By plotting the lanes (1-4), selected in (C), a histogram can be obtained for each respective lane. The barred zone of the histogram is then measured to get the area of total SHARPIN. (E) To obtain a measurement for phospho-SHARPIN, the same histogram is divided where a clear change in form of histogram can be observed. Subsequently, the barred zone of the histogram is measured to obtain a measurement of phospho-SHARPIN. The percentage of SHARPIN phosphorylation is then measured using the following formula: (Area phospho-SHARPIN/Area total SHARPIN)*100. Non-treated (1), λ-phosphatase (λPP) (2), PMA plus ionomycin (PI) (3) and PI plus λPP (4) treated CD4$^+$ cells have a phosphorylation of 31.04%, 7.58%, 78.17% and 13.32%, respectively.
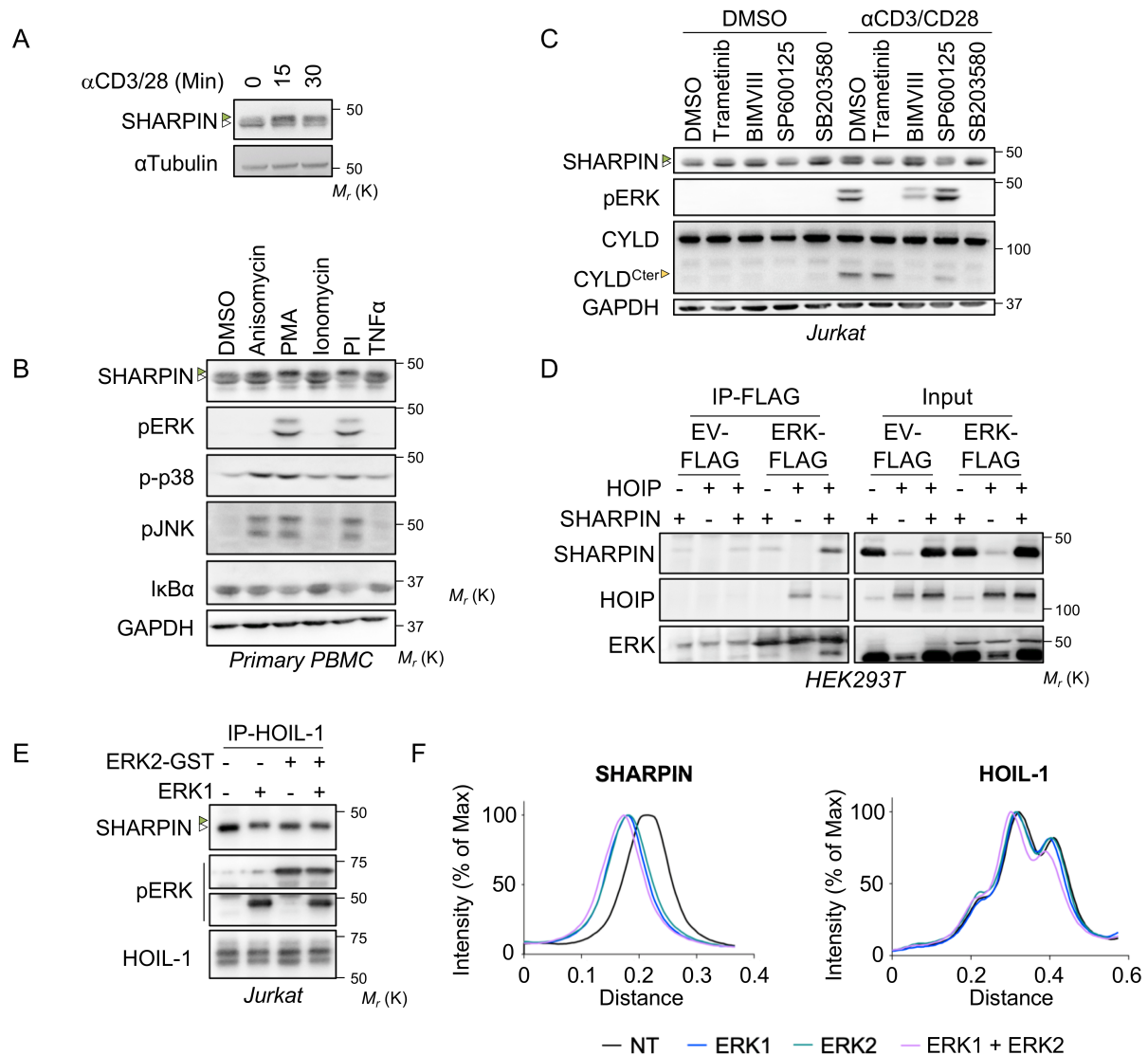
Figure S2. SHARPIN Phosphorylation by ERK upon T-cell Receptor Engagement. Related to Figure 1.

(A) Jurkat cells were stimulated with antibodies to CD3 and CD28 (1 μg/mL each) for indicated time points. Cell lysates were submitted to Western blotting analysis. Green and white arrowheads indicate phosphorylated and unphosphorylated SHARPIN, respectively. Molecular weight markers (M_r) are indicated. αTubulin was used as loading control.

(B) Primary peripheral blood mononuclear cells (PBMC) were stimulated with 12.5 μg/mL Anisomycin, 20 ng/mL PMA, 300 ng/mL ionomycin, PMA plus ionomycin (PI), or 10 ng/mL TNFα for 30 min. Cell lysates were subjected to Western blotting analysis. GAPDH served as loading control.

(C) Jurkat cells were pretreated with 1 μM Trametinib (MEK1/2 inhibitor), 500 nM Bisindolylmaleimide VIII (BIMVIII, PKC inhibitor), 50 μM SP6000125 (JNK inhibitor), or 5 μM SB203580 (p38 inhibitor), and subsequently treated with CD3 plus CD28 (1μg/μL each). Western blotting analysis was performed as indicated. Treatment with SB203580 gave non-specific results as it also regulated ERK phosphorylation. Yellow symbol indicates CYLD COOH-terminal (Cter) cleavage band, and served as a control to NF-κB activation. GADPH was used as loading control.

(D) HEK293T cells were co-transfected with plasmids encoding for HOIP, SHARPIN or HOIP plus SHARPIN together with ERK1-FLAG. Cell lysates were immunoprecipitated (IP) using anti-FLAG M2 affinity gel and subjected to Western blotting analysis. ERK served as control for pull down.

(E and F) The LUBAC was pulled down by IP of Jurkat cell lysates using the HOIL-1 antibody. *In vitro* kinase assay was performed by adding active ERK1, ERK2-GST or ERK1 plus ERK2-GST recombinant proteins to HOIL-1 pulled down beads. Western blotting analysis was performed for the indicated antibodies. HOIL-1 served as control for pull down.

A Densitometric analysis of SHARPIN and HOIL-1 blots relative to the distance of migration (Relative Distance Unit) (F) was obtained via the Plot profile function of ImageJ in the drop-down menu "Analyze". The addition of recombinant ERK led to a slower migration of SHARPIN, inducing a shift to the left in the density profile. This was however not the case for HOIL-1.

Western blotting data (A-E) are representative of three or more independent experiments.

A

Protein set	Description	Score	Peptides	Spectral Count
Sp/Q9H0F6/SHRPN_HUMAN	Sharpin OS=Homo sapiens (Human) OX=9606 GN=SHARPIN PE=1 SV=1	1048.03	20	61

B

PTM Protein Position	Pep. No.	Score	Sequence	PTM Sites Confidence	#PSM
Phospho S129	1	49.06	SNSPPALGPEACPVSLPSPPEASTLK	Phospho (S1) = 50%	3
	2	61.81	SNSPPALGPEACPVSLPSPPEASTLK	Phospho (S1) = 50% Phospho (S18) =92%	2
Phospho S131	1	49.06	SNSPPALGPEACPVSLPSPPEASTLK	Phospho (S3) = 50%	3
	2	61.81	SNSPPALGPEACPVSLPSPPEASTLK	Phospho (S3) = 50% Phospho (S18) = 92%	1
Phospho S146	3	44.59	SNSPPALGPEACPVSLPSPPEASTLK	Phospho (S18) = 91%	1
	2	61.81	SNSPPALGPEACPVSLPSPPEASTLK	Phospho (S1) = 50% Phospho (S18) = 92%	2
	2	61.81	SNSPPALGPEACPVSLPSPPEASTLK	Phospho (S3) = 50% Phospho (S18) = 92%	1
Phospho S165	4	41.63	SPGNLTER	Phospho (S1) = 100%	2
Phospho S312	5	38.87	EAPATGPSPQHPQK	Phospho (S8) = 89%	1

Figure S3. Characterization of *SHARPIN* knockout Cells. Related to figure 2.

(A) SHARPIN identified during mass spectrometry analysis (peptide rank1, peptide score > 30, FDR<1% at PSM level). The protein score is the sum of the unique peptide score calculated following -10log$_{10}$(p), where p is the absolute probability. Peptide count and spectral count are indicated.

(B) Mass spectrometry analysis of immunoprecipitates prepared from Jurkat cell lysates with antibodies to SHARPIN identified phosphorylation sites. The identified peptides were validated with an FDR < 1% and a minimum score of 30. The peptide score calculated in the Mascot search engine following -10log$_{10}$(p), where p is the absolute probability. The position of the post-translational modification in the protein (PTM), the number of peptides identified, the peptide score, the peptide sequence with the modified amino acid in blue the localization

confidence value of the post-translational modification calculated in the Mascot search engine (ptm sites confidence) and the number of spectra detected for each peptide (#PSM or peptide-spectrum match).

(C) Scheme showing the sgRNA target and PAM site on SHARPIN for the LentiCRISPR vector containing SHARPIN sgRNA.

(D) Western blotting analysis of Jurkat single cell clones targeted with sgSHARPIN LentCRISPRv2 (knock down, KD or an empty vector (EV). GAPDH was used as loading control. Molecular weight markers (M_r) are indicated.

(E) Reporter luciferase assay of Parental Jurkat and *SHARPIN* knockout (KO) cells treated for 6 h with 20 ng/mL PMA plus 300 ng/mL ionomycin, CD3 plus CD28 (1 µg/mL each) or 1 ng/mL TNFα (mean ± SEM; *P<0.05, ***P<0.001 by two-way ANOVA, compared to Parental Jurkat). Graphs represent two or three independent experiments done in triplicate.

(F) *SHARPIN* KO Jurkat cells were complemented with an empty vector (EV), or with wild-type (WT), S165A-, S312A- or S165A+S312A (2SA)-SHARPIN. Cells were stimulated for 30 min with 20 ng/mL PMA plus 300 ng/mL ionomycin. Cell lysates were subjected to Western blotting analysis. White and green symbols show SHARPIN and phosphorylated SHARPIN, respectively. αTubulin was used as loading control.

(G) Cell lysates from Jurkat, *SHARPIN* KO Jurkat cells or cells reconstituted with EV, WT-, S165A- or S165D-SHARPIN were prepared. Western blotting analysis was performed for the indicated proteins. GAPDH was used as loading control.

(H) Cell lysates from EV, WT-, S165A-, or S165D-SHARPIN reconstituted *SHARPIN* knockout Jurkat cells were subjected to SHARPIN immunoprecipitation (IP) prior to Western blotting analysis for the LUBAC components. SHARPIN served as control for pull down.

(I) SHARPIN was IP from Jurkat cell lysates. *In vitro* kinase assay was performed by adding active ERK1 plus ERK2-GST recombinant proteins. Western blotting analysis was performed with the indicated antibodies. Total SHARPIN served as control for pull down.

Western blotting data are representative of two (I), or three or more (D, F-H) independent experiments.

A

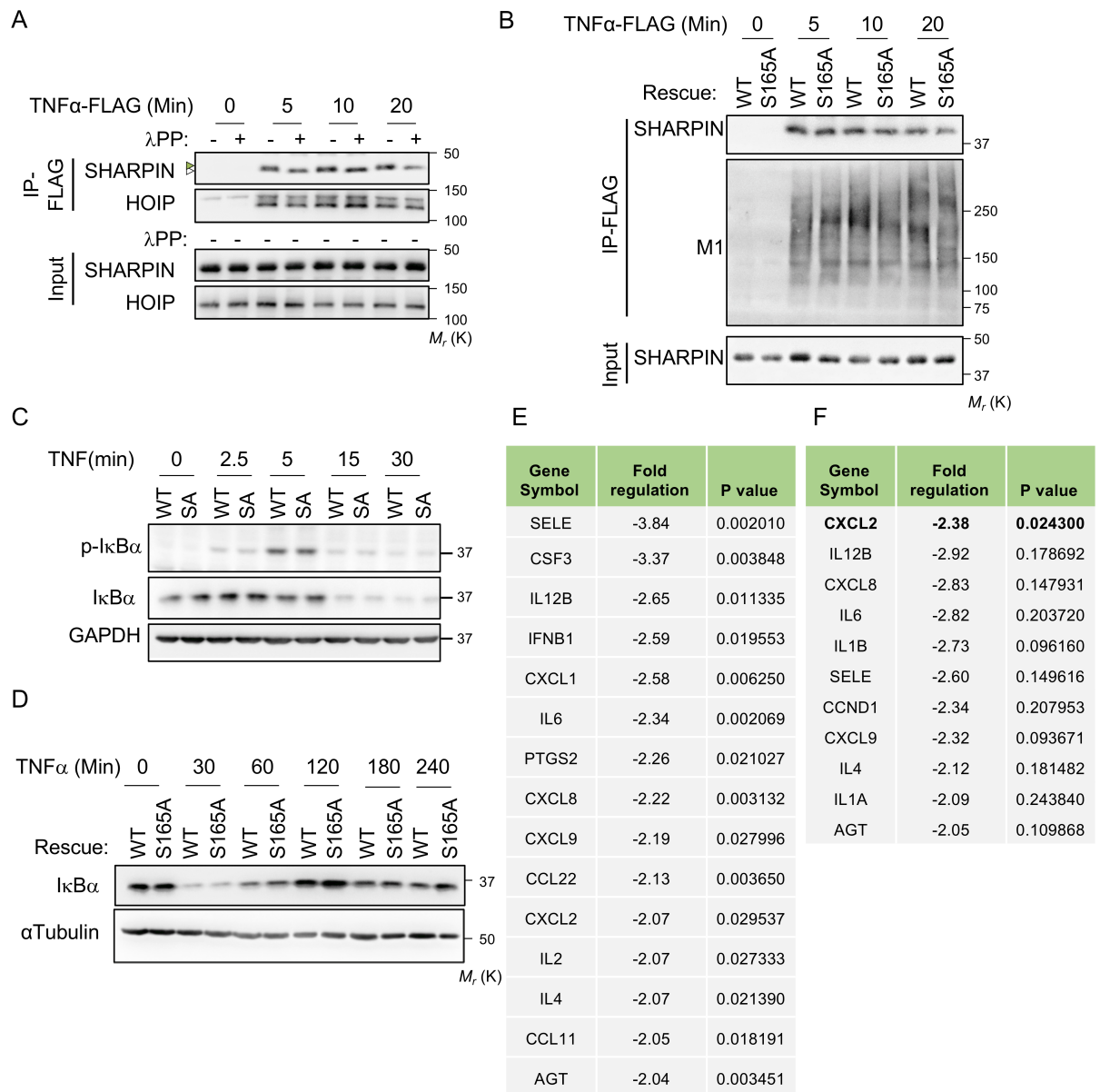TNFα-FLAG (Min) 0 5 10 20

λPP: - + - + - + - +

IP-FLAG: SHARPIN, HOIP — 50, 150, 100

λPP: - - - - - - - -

Input: SHARPIN, HOIP — 50, 150, 100

M_r (K)

B

TNFα-FLAG (Min) 0 5 10 20

Rescue: WT S165A WT S165A WT S165A WT S165A

IP-FLAG: SHARPIN — 37

M1 — 250, 150, 100, 75

Input: SHARPIN — 50, 37

M_r (K)

C

TNF(min) 0 2.5 5 15 30

WT SA WT SA WT SA WT SA WT SA

p-IκBα — 37

IκBα — 37

GAPDH — 37

D

TNFα (Min) 0 30 60 120 180 240

Rescue: WT S165A WT S165A WT S165A WT S165A WT S165A WT S165A

IκBα — 37

αTubulin — 50

M_r (K)

E

Gene Symbol	Fold regulation	P value
SELE	-3.84	0.002010
CSF3	-3.37	0.003848
IL12B	-2.65	0.011335
IFNB1	-2.59	0.019553
CXCL1	-2.58	0.006250
IL6	-2.34	0.002069
PTGS2	-2.26	0.021027
CXCL8	-2.22	0.003132
CXCL9	-2.19	0.027996
CCL22	-2.13	0.003650
CXCL2	-2.07	0.029537
IL2	-2.07	0.027333
IL4	-2.07	0.021390
CCL11	-2.05	0.018191
AGT	-2.04	0.003451

F

Gene Symbol	Fold regulation	P value
CXCL2	**-2.38**	**0.024300**
IL12B	-2.92	0.178692
CXCL8	-2.83	0.147931
IL6	-2.82	0.203720
IL1B	-2.73	0.096160
SELE	-2.60	0.149616
CCND1	-2.34	0.207953
CXCL9	-2.32	0.093671
IL4	-2.12	0.181482
IL1A	-2.09	0.243840
AGT	-2.05	0.109868

Figure S4. S165A-SHARPIN Mutant cells display reduced NF-κB Activation. Related to Figure 3.

(A and B) Jurkat cells (A) or *SHARPIN* knockout (KO) Jurkat cells, reconstituted with wild type (WT-) or S165A-SHARPIN (B) were stimulated with 100 ng/mL TNFα-FLAG for the indicated time points. Cell lysates were immunoprecipitated (IP) using anti-FLAG M2 affinity gel and subjected to Western blotting analysis. In (A), Beads were incubated with lambda phosphatase (λPP). SHARPIN and HOIP in input served as loading controls. White and green symbols show SHARPIN and phosphorylated SHARPIN, respectively. Molecular weight markers (M_r) are indicated.

(C and D) Cell lysates of WT- and S165A-expressing Jurkat were treated with 10 ng/mL TNFα for indicated time points. Western blotting analysis was performed and GAPDH or αTubulin was used as a loading control.

(E and F) List of RT² profiler PCR array of human NF-κB signaling targets with an expression fold change >2 in in cells expressing S165A-SHARPIN when compared to WT-SHARPIN. Cells were treated during 4h with 20 ng/mL PMA plus 300 ng/mL ionomycin (D) or 10 ng/mL TNFα (E). Fold regulation and p-value are listed.

Western blotting data are representative of three or more independent experiments.

Table S1. Gene list of qPCR array. Related to Figure 3.

Unigene	Refseq	Symbol	Description
Hs.441047	NM_001124	ADM	Adrenomedullin
Hs.19383	NM_000029	AGT	Angiotensinogen (serpin peptidase inhibitor, clade A, member 8)
Hs.525622	NM_005163	AKT1	V-akt murine thymoma viral oncogene homolog 1
Hs.499886	NM_000382	ALDH3A2	Aldehyde dehydrogenase 3 family, member A2
Hs.227817	NM_004049	BCL2A1	BCL2-related protein A1
Hs.516966	NM_138578	BCL2L1	BCL2-like 1
Hs.696238	NM_001166	BIRC2	Baculoviral IAP repeat containing 2
Hs.127799	NM_001165	BIRC3	Baculoviral IAP repeat containing 3
Hs.529053	NM_000064	C3	Complement component 3
Hs.54460	NM_002986	CCL11	Chemokine (C-C motif) ligand 11
Hs.303649	NM_002982	CCL2	Chemokine (C-C motif) ligand 2
Hs.534347	NM_002990	CCL22	Chemokine (C-C motif) ligand 22
Hs.514821	NM_002985	CCL5	Chemokine (C-C motif) ligand 5
Hs.523852	NM_053056	CCND1	Cyclin D1
Hs.450802	NM_000579	CCR5	Chemokine (C-C motif) receptor 5
Hs.472860	NM_001250	CD40	CD40 molecule, TNF receptor superfamily member 5
Hs.208854	NM_001781	CD69	CD69 molecule
Hs.838	NM_005191	CD80	CD80 molecule
Hs.595133	NM_004233	CD83	CD83 molecule
Hs.370771	NM_000389	CDKN1A	Cyclin-dependent kinase inhibitor 1A (p21, Cip1)
Hs.69771	NM_001710	CFB	Complement factor B
Hs.173894	NM_000757	CSF1	Colony stimulating factor 1 (macrophage)
Hs.1349	NM_000758	CSF2	Colony stimulating factor 2 (granulocyte-macrophage)
Hs.592192	NM_000395	CSF2RB	Colony stimulating factor 2 receptor, beta, low-affinity (granulocyte-macrophage)
Hs.2233	NM_000759	CSF3	Colony stimulating factor 3 (granulocyte)
Hs.789	NM_001511	CXCL1	Chemokine (C-X-C motif) ligand 1 (melanoma growth stimulating activity, alpha)
Hs.632586	NM_001565	CXCL10	Chemokine (C-X-C motif) ligand 10
Hs.75765	NM_002089	CXCL2	Chemokine (C-X-C motif) ligand 2
Hs.77367	NM_002416	CXCL9	Chemokine (C-X-C motif) ligand 9
Hs.488293	NM_005228	EGFR	Epidermal growth factor receptor
Hs.1395	NM_000399	EGR2	Early growth response 2
Hs.62192	NM_001993	F3	Coagulation factor III (thromboplastin, tissue factor)
Hs.654450	NM_000132	F8	Coagulation factor VIII, procoagulant component
Hs.667309	NM_000043	FAS	Fas (TNF receptor superfamily, member 6)
Hs.2007	NM_000639	FASLG	Fas ligand (TNF superfamily, member 6)
Hs.110571	NM_015675	GADD45B	Growth arrest and DNA-damage-inducible, beta
Hs.643447	NM_000201	ICAM1	Intercellular adhesion molecule 1
Hs.93177	NM_002176	IFNB1	Interferon, beta 1, fibroblast
Hs.856	NM_000619	IFNG	Interferon, gamma
Hs.674	NM_002187	IL12B	Interleukin 12B (natural killer cell stimulatory factor 2, cytotoxic lymphocyte maturation factor 2, p40)

Hs.168132	NM_000585	IL15	Interleukin 15
Hs.1722	NM_000575	IL1A	Interleukin 1, alpha
Hs.126256	NM_000576	IL1B	Interleukin 1, beta
Hs.25333	NM_004633	IL1R2	Interleukin 1 receptor, type II
Hs.81134	NM_000577	IL1RN	Interleukin 1 receptor antagonist
Hs.89679	NM_000586	IL2	Interleukin 2
Hs.231367	NM_000417	IL2RA	Interleukin 2 receptor, alpha
Hs.73917	NM_000589	IL4	Interleukin 4
Hs.654458	NM_000600	IL6	Interleukin 6 (interferon, beta 2)
Hs.624	NM_000584	CXCL8	Interleukin 8
Hs.700350	NM_000207	INS	Insulin
Hs.436061	NM_002198	IRF1	Interferon regulatory factor 1
Hs.36	NM_000595	LTA	Lymphotoxin alpha (TNF superfamily, member 1)
Hs.376208	NM_002341	LTB	Lymphotoxin beta (TNF superfamily, member 3)
Hs.463978	NM_002758	MAP2K6	Mitogen-activated protein kinase kinase 6
Hs.297413	NM_004994	MMP9	Matrix metallopeptidase 9 (gelatinase B, 92kDa gelatinase, 92kDa type IV collagenase)
Hs.202453	NM_002467	MYC	V-myc myelocytomatosis viral oncogene homolog (avian)
Hs.82116	NM_002468	MYD88	Myeloid differentiation primary response gene (88)
Hs.592142	NM_181659	NCOA3	Nuclear receptor coactivator 3
Hs.618430	NM_003998	NFKB1	Nuclear factor of kappa light polypeptide gene enhancer in B-cells 1
Hs.73090	NM_002502	NFKB2	Nuclear factor of kappa light polypeptide gene enhancer in B-cells 2 (p49/p100)
Hs.81328	NM_020529	NFKBIA	Nuclear factor of kappa light polypeptide gene enhancer in B-cells inhibitor, alpha
Hs.406515	NM_000903	NQO1	NAD(P)H dehydrogenase, quinone 1
Hs.563344	NM_006186	NR4A2	Nuclear receptor subfamily 4, group A, member 2
Hs.1976	NM_002608	PDGFB	Platelet-derived growth factor beta polypeptide
Hs.77274	NM_002658	PLAU	Plasminogen activator, urokinase
Hs.196384	NM_000963	PTGS2	Prostaglandin-endoperoxide synthase 2 (prostaglandin G/H synthase and cyclooxygenase)
Hs.633256	NM_002908	REL	V-rel reticuloendotheliosis viral oncogene homolog (avian)
Hs.502875	NM_021975	RELA	V-rel reticuloendotheliosis viral oncogene homolog A (avian)
Hs.654402	NM_006509	RELB	V-rel reticuloendotheliosis viral oncogene homolog B
Hs.82848	NM_000450	SELE	Selectin E
Hs.73800	NM_003005	SELP	Selectin P (granule membrane protein 140kDa, antigen CD62)
Hs.167317	NM_003081	SNAP25	Synaptosomal-associated protein, 25kDa
Hs.487046	NM_000636	SOD2	Superoxide dismutase 2, mitochondrial
Hs.642990	NM_007315	STAT1	Signal transducer and activator of transcription 1, 91kDa
Hs.463059	NM_003150	STAT3	Signal transducer and activator of transcription 3 (acute-phase response factor)
Hs.595276	NM_012448	STAT5B	Signal transducer and activator of transcription 5B
Hs.241570	NM_000594	TNF	Tumor necrosis factor
Hs.256278	NM_001066	TNFRSF1B	Tumor necrosis factor receptor superfamily, member 1B
Hs.478275	NM_003810	TNFSF10	Tumor necrosis factor (ligand) superfamily, member 10
Hs.437460	NM_000546	TP53	Tumor protein p53

Hs.522506	NM_021138	TRAF2	TNF receptor-associated factor 2
Hs.109225	NM_001078	VCAM1	Vascular cell adhesion molecule 1
Hs.356076	NM_001167	XIAP	X-linked inhibitor of apoptosis
Hs.520640	NM_001101	ACTB	Actin, beta
Hs.534255	NM_004048	B2M	Beta-2-microglobulin
Hs.592355	NM_002046	GAPDH	Glyceraldehyde-3-phosphate dehydrogenase
Hs.412707	NM_000194	HPRT1	Hypoxanthine phosphoribosyltransferase 1
Hs.546285	NM_001002	RPLP0	Ribosomal protein, large, P0

TRANSPARENT METHODS

Cell Culture and Stimulation

Jurkat E6.1 T lymphocytes, Hela, HEK293T and MCF7 cells were purchased from American Type Culture Collection (ATCC). U2932, SUDHL4, BJAB, RIVA, OCI-LY3, and OCI-LY19 cells were acquired from DSMZ. HBL1, HLY1 and TMD8 cells were kindly provided by Martin Dyer, Pierre Brousset, and Daniel Krappmann, respectively. Blood was obtained from healthy donors (Etablissement Français du Sang). Peripheral blood mononuclear cells (PBMC) were acquired by Ficoll density gradient. Primary $CD4^+$ and $CD8^+$ T cells were subsequentially isolated from PBMC using REAlease CD4 and CD8 microbeads kits, from Miltenyi as manufacturer's instructions. Cell viability was assessed using CellTiter-Glo following manufacturer's instructions (Promega) following stimulation with 10 ng/mL TNFα (R&D systems) for 24h. Jurkat E6.1, PBMC or primary T cells were stimulated with 20 ng/mL Phorbol 12-Myristate 13 Acetate (PMA, Merck), 300 ng/mL ionomycin (Merck), PMA plus ionomycin, 1 μg/mL CD3 plus 1 μg/mL CD28 (Becton Dickinson Biosciences), 12.5 mg/mL Anisomycin (Merck), 10 ng/mL TNFα (R&D systems) or TNFα-Flag (Enzo Life Sciences). To ensure inhibition of certain signaling pathways, Jurkat, PBMC or primary T cells were pre-treated during 1h with 1 μM Trametinib (Selleckchem), 500 nM Bisindolylmaleimide VIII (BIMVIII, Enzo), 50 μM SP6000125 (Cell Signaling), or 5 μM SB203580 (Selleckchem).

Immunoblotting

Cells were washed with ice-cold PBS and subsequently lysed with TNT buffer (50 mM Tris-HCl (pH 7.4), 150 mM NaCl, 1% Triton X-100, 1% Igepal, 2 mM EDTA) supplemented with 1x Halt Protease Inhibitor cocktail (ThermoFisher Scientific), and incubated for 30 min on ice. Extracts were cleared by centrifugation at >10,000x*g*. To obtain cytosolic and nuclear fractions,

cells pellets were incubated with 188 μl of Buffer A (10 mM HEPES pH7.9, 10 mM KCL, 0.1 mM EDTA, 0.1 mM EGTA, 1mM DTT, 1 mM Na_3VO_4, and Protease Inhibitors) for 5 min on

ice. 12 μl of Buffer A containing 10% Igepal was added for another 5 min on ice and samples were subsequently centrifuged at 1,000xg for 3 min. Supernatant was collected and further spun at 25,000xg to obtain a cytosolic fraction. Nuclei were washed with Buffer A and lysed with 30 μl of Buffer C (20 mM HEPES pH7.9, 400 mM NaCl, 1 mM EDTA, 1 mM EGTA, 1 mM DTT, 1 mM Na_3VO_4, and Protease Inhibitors) and cleared by a >10,000xg centrifugation. Protein concentration was determined using the Micro BCA Protein Assay kit (ThermoFisher scientific). Lambda phosphatase experiments used either Buffer A or TNT lysis without EDTA or EGTA for cell lysis. 10 μg of proteins were incubated with 600 Units of lambda phosphatase, 1x NEB buffer for Protein Metallophosphatase and 1mM $MnCl_2$ (New England Biolabs) for 30 min at 30°C. 10 µg of proteins were incubated with 2X Laemmli buffer (Life Technologies) at 95°C for 3 min, separated by SDS-PAGE using 3-15% Tris-Acetate gels and transferred to nitrocellulose membranes (GE Healthcare). Phos-tag gels were purchased from FUJIFILM Wako Pure Chemical cooperation. In brief, 100,000 Jurkat cells stimulated with 20 ng/mL PMA plus 300 ng/mL ionomycin for 30 min were lysed directly with 25 µl of Laemmli buffer and boiled for 10 min. 1 mM of $ZnCl_2$ was added to the samples prior to running on the Phos-tag gel. Gel was washed in transfer buffer (Biorad) containing 10 mM EDTA (Sigma) before transferring to nitrocellulose membranes and Western blotting analysis.

Densitometry analysis was performed by the Image J software (National Institutes of Health). In short, the gels function of Image J was used to identify, plot and analyze lanes of interest. By plotting lanes, a histogram can be obtained for the entire protein of interest. To obtain measurements for phospho-SHARPIN, the same histogram is divided where a clear change in histogram form can be observed. The percentage of SHARPIN phosphorylation is calculated by the following formula: (Area phospho-SHARPIN/Area total SHARPIN) x 100 (Figures S1C-E).

The following antibodies were used for analysis by immunoblot: SHARPIN (A303-559A) and HOIP (A303-560A) antibodies were purchased from Bethyl Laboratories. HOIL-1 (sc-

393754), αTubulin (sc-8035), CYLD (sc-137139), GAPDH (sc-32233) and PARP (sc-8007) antibodies were obtained from Santa Cruz Biotechnology. Phospho-ERK (#9106), IκBα (#9242), OTULIN (#14127), phospho-IκBα (#9246), phospho-p38 (#9215), phospho-JNK (#9255) and RIP1 (#3493) were acquired from Cell Signaling Technologies. Anti-linear Ubiquitin were procured from Millipore (MABS199) or from Genentech (Matsumoto et al., 2012). NEMO antibody (559675) was purchased from BD Biosciences. For detection of the phospho-S165 from of human SHARPIN, five Balb/C mice were primed via intraperitoneal injection with complete Freund adjuvant and boosted two times at two-week intervals with incomplete Freund adjuvant with a synthetic phosphorylated peptide (DLPR(Sp)PGNLTERC) conjugated to KLH. Mouse blood was collected from the submandibular vein and serum reactivity was confirmed by ELISA with phosphorylated and non-phosphorylated biotinylated peptide. Mouse serum was used to reveal phospho-S165 SHARPIN.

Immunoprecipitation and ERK Recombinant Kinase Assay

Cells were washed with ice-cold PBS, lysed with TNT buffer and incubated for 30 min on ice. Extracts were cleared by centrifugation at >10,000x*g*. Protein concentration was determined using the Micro BCA protein kit. Samples were precleared with Protein G Sepharose (Merck) for 30 min, and subsequently incubated with 1 µg of antibody and protein G Sepharose for 2h. FLAG pull down was performed incubating cleared cell lysates with Anti-FLAG M2 affinity gel (Merck) during 2h. Antibodies to SHARPIN (A303-559A, Bethyl), HOIL-1 (sc-393754, Santa Cruz Biotechnology) and linear ubiquitin (Genentech, (Matsumoto et al., 2012)) were used for IP. For NEMO ubiquitination, samples were lysed with buffer containing 1% SDS and heated at 90°C to detach non-covalently bound proteins. SDS was subsequently diluted to 0.1% prior IP with antibodies against NEMO (sc-8330, Santa Cruz Biotechnology). ERK1/2 kinase assay was performed from beads immunoprecipitated for HOIL-1 or SHARPIN. Beads were washed in kinase buffer (5 mM MOPS pH 7.2, 2.5 mM Glycerol 2-phosphate, 5 mM MgCl$_2$, 1 mM EGTA, 0.4 mM EDTA, 0.05 mM DTT). Beads were subsequently incubated

with kinase buffer, 2mM ATP, 350 ng/mL active untagged ERK1 (Merck), 350 ng/mL active ERK2-GST tagged (Merck) or 175 ng/mL ERK1 plus 175 ng/mL ERK2-GST for 30 min at 30°C. Lambda phosphatase experiments using TNT buffer without EDTA were performed as described above.

Mass Spectrometry

The immunoprecipitation of SHARPIN was performed in Jurkat E6.1 cells, as described above. Proteins were separated by SDS-PAGE. The Colloidal Blue Staining kit (LC6025, Invitrogen) was used to stain protein as per manufacturer's instructions. Gel was excised between 37 and 50 kDa, to ensure the presence of SHARPIN, and subsequently cut into smaller fragments. Fragments were washed alternating between 100 mM Ammonium Bicarbonate and Acetonitrile. Disulfide bonds of proteins were reduced, with using 65 mM DTT for 15 min at 37°C, and subsequently alkylated by 135 mM Iodoacetamide for 15 min at room temperature. Enzymatic digestion of proteins was performed at 37°C overnight by incubating the gel pieces in 25 ng/mL pH 8.5 trypsin solution (Sequenced Grade Modified Trypsin, ref V511A, Porcine, Promega). Digested peptides were extracted by incubation in 70% and 100% acetonitrile for 20 min each. Peptide extracts were evaporated and afterward reconstituted in 0.1% formic acid. Peptide extracts were analyzed by liquid nano-chromatography (nanoLC) nanoElute coupled with a TimsTOF Pro mass spectrometer (Bruker) (Banliat et al., 2020). Generated peaks were analyzed with the Mascot database search engine (MatrixScience version 2.5.01) for peptide and protein identification. The peaks were queried simultaneously in the: UniprotKB Human (release 20191016, 20656 sequences) database and a decoy database that was interrogated in parallel to estimate the number of false identifications and to calculate the threshold at which the scores of the identified peptides are valid. Mass tolerance for MS and MS/MS was set at 15 ppm and 0.05 Da, respectively. The enzyme selectivity was set to full trypsin with one miscleavage allowed. Protein modifications were fixed carbamidomethylation of cysteines, variable oxidation of methionine, variable phosphorylation of serine, threonine or tyrosine. Identified proteins are

validated with an FDR < 1% at PSM level and a peptide minimum score of 30, using Proline v2.0 software (Bouyssié et al., 2020). Proteins identified with the same set of peptides are automatically grouped together. Analysis of post-translational modifications was also executed using Proline v2.0 Software. Localization confidence values for peptide ions were exported from Mascot (Savitski et al., 2011) and a site probability is calculated for a particular modification according to the number of peptides confidently detected with this site modification.

CRISPR/Cas9 knock out and SHARPIN reconstituted Cell Lines

LentiGuide and LentiCRISPRv2 vectors (GeCKO, ZhangLab), were cloned to contain SHARPIN guide RNA (5' CACCGTGGCTGTGCACGCCGCGGTG 3') (Sanjana et al., 2014; Shalem et al., 2014). LentiCRISPRv2, together with the packaging vectors PAX2 and VSV-G, were transfected in HEK293T cells using a standard calcium phosphate protocol (Douanne et al., 2019). Supernatant, containing the lentiviral particles, was collected after 48 h, and used to infect 10^6 Jurkat cells in presence of 8 μg/mL Polybrene (Santa Cruz Biotechnology). Jurkat cells expressing the LentiCRISPRv2 vector were selected by adding 1μg/mL Puromycin to their media, and subsequently dilution cloned. Single-cell clones were then picked and tested for functional Cas9 cutting of SHARPIN (Figure S3C). pCMV3flag8SHARPIN was a gift from Martin Dorf (Addgene plasmid #50014; http://n2t.net/addgene:50014; RRID:Addgene_50014) and served to clone SHARPIN into a pCMH-MSCV-EF1a-puroCopGFP vector (SBI). Site directed mutagenesis was performed to substitute the serine (S) residues on 165 or/and 312 to an alanine (A) or an aspartic acid (D). CRISPR/Cas9 resistance was achieved by site directed mutagenesis of the PAM sequence on site 29, substituting an Arginine (AGG) to an Arginine (AGA).

NF-κB Assays

NF-κB luciferase assays were measured 6 h post-stimulation, following the manufacturer's instruction (Promega) (Douanne et al., 2016; Dubois et al., 2014). DNA binding of the NF-κB subunits was measured using TransAM NF-κB activation assay (Actif Motif), as per manufacturer's instructions. *SHARPIN* knockout Jurkat cells reconstituted with WT- or S165A-SHARPIN were treated with 20 ng/mL PMA plus 300 ng/mL Ionomycin or 10 ng/mL TNFα during 30 min prior to TransAM experiment. For the RT^2 profiler PCR array of human NF-κB signaling targets, cells were treated with 20 ng/mL PMA plus 300 ng/mL Ionomycin or 10 ng/mL TNFα for 4h. RNA was extracted using the Nucleospin RNAplus kit (Macherey-Nagel), following manufacturer's instructions. 2 μg of RNA was reverse transcribed using the Maxima Reverse Transcriptase kit (ThermoFisher). RT^2 profiler PCR array of human NF-κB signaling targets was performed as instructed by the manufacturer (PAHS-225Z, Qiagen). The gene list can be found in table S1.

Statistical Analysis

Statistical analysis, comparing multiple groups was performed using two-way ANOVA on rank test with Tuckey's post hoc test in GraphPad Prism 7 software. TransAM NF-κB activation assays were analyzed using a 2-way ANOVA test with a Sidak correction for multiple analysis. RT^2 profiler PCR array was performed using the online software provided by the manufacturer (https://dataanalysis2.qiagen.com/pcr). In short, the p-values were calculated based on a student t-test of the replicate $2^{\wedge}(-DC_T)$ values for each gene in the control group and treatment group. The p-value calculation used is based on a parametric, unpaired, two sample equal variance, two-tailed distribution. P-values < 0.05 were considered as significant.

SUPPLEMENTAL REFERENCES

Banliat, C., Tsikis, G., Labas, V., Teixeira-Gomes, A.-P., Com, E., Lavigne, R., Pineau, C., Guyonnet, B., Mermillod, P., and Saint-Dizier, M. (2020). Identification of 56 Proteins Involved in Embryo–Maternal Interactions in the Bovine Oviduct. Int. J. Mol. Sci. *21*, 466.

Bouyssié, D., Hesse, A.-M., Mouton-Barbosa, E., Rompais, M., Macron, C., Carapito, C., Gonzalez de Peredo, A., Couté, Y., Dupierris, V., Burel, A., et al. (2020). Proline: an efficient and user-friendly software suite for large-scale proteomics. Bioinformatics *36*, 3148–3155.

Douanne, T., Gavard, J., and Bidère, N. (2016). The paracaspase MALT1 cleaves the LUBAC subunit HOIL1 during antigen receptor signaling. J. Cell Sci. *129*, 1775–1780.

Douanne, T., André-Grégoire, G., Trillet, K., Thys, A., Papin, A., Feyeux, M., Hulin, P., Chiron, D., Gavard, J., and Bidère, N. (2019). Pannexin-1 limits the production of proinflammatory cytokines during necroptosis. EMBO Rep. *20*, e47840.

Dubois, S.M., Alexia, C., Wu, Y., Leclair, H.M., Leveau, C., Schol, E., Fest, T., Tarte, K., Chen, Z.J., Gavard, J., et al. (2014). A catalytic-independent role for the LUBAC in NF-kappaB activation upon antigen receptor engagement and in lymphoma cells. Blood *123*, 2199–2203.

Matsumoto, M.L., Dong, K.C., Yu, C., Phu, L., Gao, X., Hannoush, R.N., Hymowitz, S.G., Kirkpatrick, D.S., Dixit, V.M., and Kelley, R.F. (2012). Engineering and structural characterization of a linear polyubiquitin-specific antibody. J. Mol. Biol. *418*, 134–144.

Savitski, M.M., Lemeer, S., Boesche, M., Lang, M., Mathieson, T., Bantscheff, M., and Kuster, B. (2011). Confident Phosphorylation Site Localization Using the Mascot Delta Score. Mol. Cell. Proteomics *10*, M110.003830.